Article

Cell

Circuit Architecture of VTA Dopamine Neurons Revealed by Systematic Input-Output Mapping

Graphical Abstract

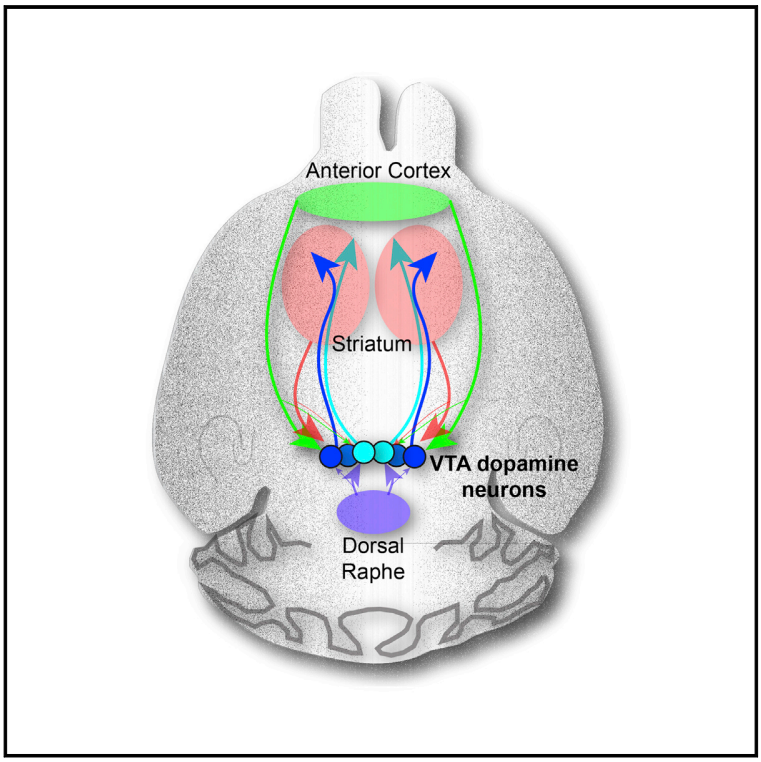

Authors

Kevin T. Beier, Elizabeth E. Steinberg, Katherine E. DeLoach, ..., Eric J. Kremer, Robert C. Malenka, Liqun Luo

Correspondence

malenka@stanford.edu (R.C.M.), lluo@stanford.edu (L.L.)

In Brief

A combination of state-of-the-art viral-genetic tools shows that dopaminergic neurons in the ventral tegmental area (VTA-DA) employ biased-input/discrete-output circuit architecture, allowing the construction of an input-output map for further investigation of the neural circuits underlying the different functions of these neurons in psychological processes and brain diseases.

Highlights

- VTA dopamine (DA) and GABA neurons receive similar inputs from diverse sources
- VTA-DA neurons projecting to different output sites receive biased input
- VTA-DA neurons projecting to lateral and medial NAc innervate non-overlapping targets
- A top-down anterior cortex → VTA-DA → lateral NAc circuit is reinforcing

Beier et al., 2015, Cell *162*, 622–634
July 30, 2015
http://dx.doi.org/10.1016/j.cell.2015.07.015

CellPress

Cell

Article

Circuit Architecture of VTA Dopamine Neurons Revealed by Systematic Input-Output Mapping

Kevin T. Beier,[1,2] Elizabeth E. Steinberg,[2] Katherine E. DeLoach,[1] Stanley Xie,[1] Kazunari Miyamichi,[1,5] Lindsay Schwarz,[1] Xiaojing J. Gao,[1,6] Eric J. Kremer,[3,4] Robert C. Malenka,[2,*] and Liqun Luo[1,*]

[1]Howard Hughes Medical Institute and Department of Biology, Stanford University, Stanford, CA 94305, USA

[2]Nancy Pritzker Laboratory, Department of Psychiatry and Behavioral Sciences, Stanford University School of Medicine, Stanford, CA 94305, USA

[3]Institut de Génétique Moléculaire de Montpellier, CNRS 5535, 34293 Montpellier, France

[4]Université de Montpellier, 34000 Montpellier, France

[5]Present address: Department of Applied Biological Chemistry, Graduate School of Agricultural and Life Sciences, The University of Tokyo, Tokyo 113-8657, Japan

[6]Present address: Division of Biology, California Institute of Technology, Pasadena, CA 91125, USA

*Correspondence: malenka@stanford.edu (R.C.M.), lluo@stanford.edu (L.L.)

http://dx.doi.org/10.1016/j.cell.2015.07.015

SUMMARY

Dopamine (DA) neurons in the midbrain ventral tegmental area (VTA) integrate complex inputs to encode multiple signals that influence motivated behaviors via diverse projections. Here, we combine axon-initiated viral transduction with rabies-mediated trans-synaptic tracing and Cre-based cell-type-specific targeting to systematically map input-output relationships of VTA-DA neurons. We found that VTA-DA (and VTA-GABA) neurons receive excitatory, inhibitory, and modulatory input from diverse sources. VTA-DA neurons projecting to different forebrain regions exhibit specific biases in their input selection. VTA-DA neurons projecting to lateral and medial nucleus accumbens innervate largely non-overlapping striatal targets, with the latter also sending extensive extra-striatal axon collaterals. Using electrophysiology and behavior, we validated new circuits identified in our tracing studies, including a previously unappreciated top-down reinforcing circuit from anterior cortex to lateral nucleus accumbens via VTA-DA neurons. This study highlights the utility of our viral-genetic tracing strategies to elucidate the complex neural substrates that underlie motivated behaviors.

INTRODUCTION

Dopamine (DA) neuron dysfunction has been implicated in numerous brain disorders, including addiction, depression, schizophrenia, and Parkinson's disease. Our incomplete understanding of the complex brain circuits in which dopamine neurons participate represents a major obstacle to developing more sophisticated hypotheses and improved treatments for these disorders. In the mammalian brain, the majority of DA neurons are clustered in two adjacent midbrain regions, the ventral tegmental area (VTA) and substantia nigra pars compacta (SNc). Initial in vivo electrophysiological studies suggested that midbrain DA neurons were a homogenous population, uniformly excited by rewards or reward-predictive cues and unaffected or transiently inhibited by aversive events (Mirenowicz and Schultz, 1996; Ungless et al., 2004). These findings were consistent with behavioral evidence demonstrating an unequivocal relationship between DA transmission and the reinforcing effects of natural and drug rewards (Wise and Rompré, 1989). However, the simplifying assumption that DA neurons functioned as a homogenous unit was called into question as data emerged that were inconsistent with this account. Although most DA neurons were activated by reward and reward-predictive cues, some were activated by noxious or salient stimuli (Brischoux et al., 2009; Matsumoto and Hikosaka, 2009; Zweifel et al., 2011). Furthermore, important roles for DA neurons were uncovered in numerous behavioral or psychological processes other than reward, including salience, aversion, fear, working memory, and movement coordination (Bromberg-Martin et al., 2010; Jin and Costa, 2010; Zweifel et al., 2011; Lammel et al., 2012; Matsumoto and Takada, 2013). Heterogeneity was also detected at the cellular level, as subpopulations of DA neurons were found to have distinct intrinsic molecular and electrophysiological properties (Margolis et al., 2006a, 2008; Lammel et al., 2008, 2011).

Although a consensus is emerging that DA neurons are best conceptualized as functionally heterogeneous subpopulations capable of influencing diverse behavioral states (Bromberg-Martin et al., 2010; Roeper, 2013; Marinelli and McCutcheon, 2014), the underlying organizational principles that account for this heterogeneity remain unclear. Such principles would be especially useful in understanding the function of the VTA, which is cytochemically more diverse than the SNc (Margolis et al., 2006b). In addition to DA neurons, the VTA contains neurons that release GABA, glutamate, and their various combinations, all of which form local and long-range connections (Swanson, 1982; Fields et al., 2007; Morales and Root, 2014; Root et al., 2014). The anatomical location of a DA neuron's synaptic inputs and/or outputs may be a key determinant of its intrinsic properties and behavioral roles (Lammel et al., 2008; Margolis et al., 2008; Lammel et al., 2011, 2012). Thus, a comprehensive map detailing

both the input and output connections of VTA-DA neurons would be of great value in deducing principles of midbrain circuit function.

Previous studies have sought to separately identify either the sources of synaptic inputs to VTA neurons (Phillipson, 1979; Carr and Sesack, 2000; Zahm et al., 2011; Watabe-Uchida et al., 2012) or the projection targets of these cells (Beckstead et al., 1979; Swanson, 1982). However, these experiments have two major limitations. First, synaptic inputs to the two main classes of VTA neurons (DA and GABA neurons) have not been comparatively evaluated at the whole-brain level. VTA-DA and VTA-GABA neurons have distinct firing patterns in vivo (Cohen et al., 2012), and their optogenetic activation produces opposing behavioral effects (Tsai et al., 2009; Tan et al., 2012). Thus, a systematic, comparative analysis of synaptic input onto VTA-DA and VTA-GABA neurons could be informative in elucidating general organizational principles that permit interdigitated neurons to make distinct contributions to brain function.

A second limitation has been an inability to systematically link information about a VTA-DA neuron's inputs with its projection targets. Although such input-output relationships can be established in ultrastructural studies (e.g., Carr and Sesack, 2000), the methods involved are labor intensive and thus cannot practically be scaled up to elucidate whole-brain input-output maps. Accordingly, only a handful of three-node circuits involving VTA neurons have been identified, undoubtedly representing a small fraction of such connections.

To address these limitations, we utilized rabies virus-based and cell-type-specific monosynaptic tracing techniques (Wickersham et al., 2007; Callaway and Luo, 2015), as well as a viral-genetic strategy that permits whole-brain mapping of input-output relationships of genetically defined neuronal populations (Schwarz et al., 2015). These methods allowed for the generation of a comprehensive, high-resolution map of the input and output connectivity of VTA-DA neurons, thereby revealing previously unappreciated connections, including an anterior cortex→VTA-DA→nucleus accumbens (NAc) circuit. Using optogenetics, electrophysiology, and in vivo pharmacology, we verify the functional relevance of this circuit by demonstrating its role in positive reinforcement. Collectively, our data demonstrate that the input-output relationships of VTA-DA neuron subpopulations are complex yet decipherable. They provide a critical roadmap for the development of more sophisticated and testable hypotheses about the neural circuit substrates that mediate the diverse behavioral functions of the VTA, in particular its DA neurons, in adaptive and pathological behaviors.

RESULTS

VTA-DA and VTA-GABA Neurons Receive Direct Input from Similar Brain Regions

Rabies-mediated trans-synaptic tracing has previously been used to map direct inputs to DA neurons in two major midbrain nuclei, the SNc and VTA (Watabe-Uchida et al., 2012). To comprehensively map input and output through the VTA, we first extended these studies by comparing direct inputs to both VTA-DA and VTA-GABA neurons and then examined the cell types in the input regions that synapse onto these two VTA populations.

To restrict our analysis specifically to VTA-DA and VTA-GABA neurons, we used *DAT-Cre* mice, in which Cre mimics the expression pattern of the plasma membrane dopamine transporter (Bäckman et al., 2006; Lammel et al., 2015), and *GAD2-Cre* mice, in which Cre mimics the expression of glutamic acid decarboxylase-2 (Taniguchi et al., 2011), an enzyme that coverts glutamate to GABA (Figure S1). Two adeno-associated viruses (AAVs), expressing, respectively, a Cre-dependent TVA (the receptor for viruses containing the avian EnvA envelope glycoprotein) fused with mCherry (TC) and a Cre-dependent rabies glycoprotein (G), were injected into the VTA of these mice (Figure 1A) (Miyamichi et al., 2013). Two weeks later, we injected EnvA-pseudotyped, *G*-deleted, and GFP-expressing rabies virus (RV*dG*). RV*dG* could only infect TC-expressing mammalian cells due to the EnvA pseudotype. Co-expression of *G* enabled TC-expressing neurons to complement RV*dG* and produce infectious rabies viruses that spread to their presynaptic partners. Almost all starter cells (defined by co-expression of TC and GFP) in the *DAT-Cre* mice expressed tyrosine hydroxylase (TH, a marker for DA neurons) (Figure 1B; quantified in Figure 1P, inset), whereas few starter cells in the VTA of *GAD2-Cre* mice co-expressed TH (Figure 1C; quantified in Figure 1P, inset). Control experiments demonstrated that the rabies-mediated trans-synaptic tracing depended on Cre recombinase, TC, and G expression (Figure S2). Together, these results validated the cell-type specificity for input tracing.

We comparatively evaluated the sources of synaptic inputs to VTA-DA and VTA-GABA neurons by examining the distribution of GFP-positive neurons across different brain regions. Consistent with previous results (Watabe-Uchida et al., 2012), VTA-DA (Figures 1D–1O) and VTA-GABA (data not shown) neurons received direct synaptic inputs from diverse neuronal types in a wide range of brain regions. We quantified input neurons in 22 brain regions (see Supplemental Experimental Procedures for details) and calculated the proportion of inputs from each region for both *DAT-Cre*- and *GAD2-Cre*-based tracing (Figure 1P and Table S1). VTA-GABA neurons received proportionally more inputs from the anterior cortex and central amygdala (CeA), whereas VTA-DA neurons received more inputs from the paraventricular hypothalamus (PVH) and lateral hypothalamus (LH), although none of these differences were significant when corrected for multiple comparisons. These results suggest that VTA-DA and VTA-GABA neurons receive largely similar input from different brain regions.

VTA-DA and VTA-GABA Neurons Receive Input from Diverse Cell Types

To explore whether differences may exist at the cellular level within each input region, we combined in situ hybridization (ISH) with rabies tracing (Takatoh et al., 2013; Weissbourd et al., 2014) on three selected input regions: the PVH, LH, and dorsal raphe (DR), each of which contains heterogeneous neuronal populations that are implicated in reward-related behaviors.

In the PVH (Figure 2A), we used probes for genes encoding the precursors for the neuropeptides oxytocin and arginine vasopressin (AVP), which have been implicated in several behavioral processes, including reward, fear, and anxiety (Stoop, 2012). However, it is unknown whether neurons producing these

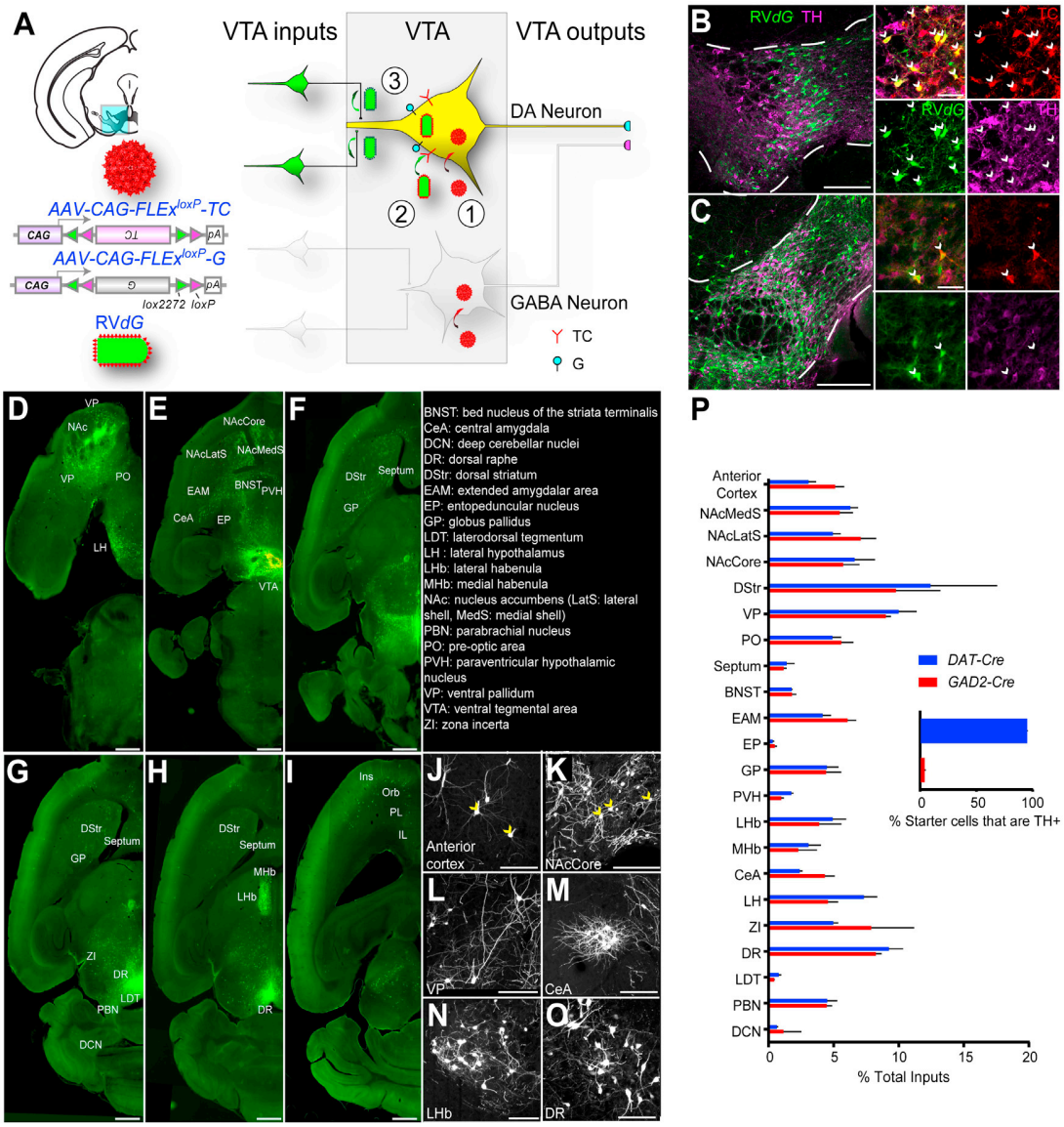

Figure 1. Rabies-Mediated Trans-synaptic Tracing Reveals Inputs to VTA-DA and -GABA Neurons

(A) Schematic of rabies tracing, shown for *DAT-Cre*. Left, diagrams of the injection site (blue box highlights the VTA) and the viruses used. (1) Injections of AAVs expressing Cre-dependent TVA-mCherry (TC) and rabies glycoprotein (G) were targeted unilaterally to the VTA. (2) Two weeks later, EnvA-pseudotyped, G-deleted, GFP-expressing rabies virus (RV*dG*) was injected into the same VTA site. (3) Five days were allowed for rabies to transduce and label synaptically connected input neurons.

(B and C) In the VTA (between the dotted lines), most TC-expressing cells in *DAT-Cre* mice co-stained with the anti-tyrosine hydroxylase (TH) antibody (B), while TC-labeled cells in *GAD2-Cre* animals did not (C). In the insets, arrows indicate TC-expressing cells. Green, GFP from RV*dG*; red, TC; magenta, TH immunoreactivity. Scale, 200 μm (100 μm for inset).

(D–I) Horizontal section series showing brain-wide distribution of input to VTA-DA neurons. Scale, 1 mm.

(J–O) High-magnification images of rabies-infected input neurons, including principal neurons in the cortex and striatal projection neurons in the NAcCore (yellow arrowheads). Scale, 100 μm.

(P) Quantification of inputs to VTA-DA or VTA-GABA neurons from *DAT-Cre* or *GAD2-Cre* mice, respectively. Data are shown as percent of inputs from a given region relative to total counted inputs throughout a given brain. Although overall inputs to DA and GABA neurons are significantly different ($p < 0.01$, Fisher's combined probability test), no individual input showed a significant preference for DA or GABA neurons ($p > 0.05$ for all inputs, t test with Holm-Sidak correction for multiple comparisons). Inset, 95% of starter cells in the VTA of *DAT-Cre* mice are TH^+, whereas 4% in *GAD2-Cre* animals are TH^+; n = 4 for each condition. In this and all subsequent figures, error bars represent SEM.

See also Figure S1, S2, S4, and S5 and Tables S1, S2, and S3 for related data.

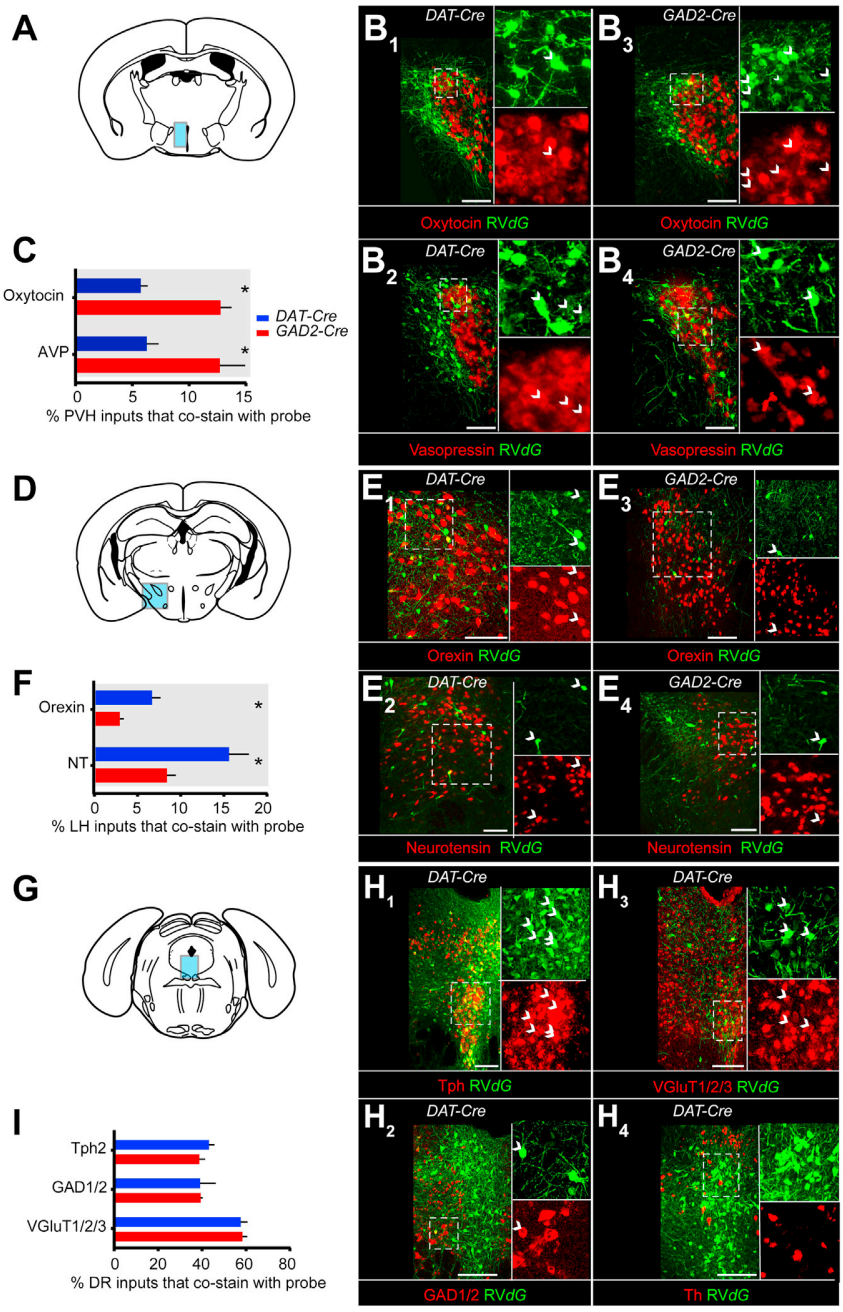

Figure 2. VTA-DA and VTA-GABA Neurons Receive Synaptic Inputs from Diverse Cell Types

(A) Coronal schematic showing the PVH (blue), where inputs to VTA-DA and -GABA neurons were examined for expression of the mRNAs encoding either oxytocin (B_1, B_3) or arginine vasopressin (AVP; B_2, B_4) precursors.

(B) Overlap of ISH signals (red) with GFP from RV*dG* (green) was observed for inputs to both VTA-DA (B_1–B_2) and VTA-GABA (B_3–B_4) neurons. Arrowheads indicate cells co-labeled with ISH probe and GFP.

(C) Quantification of percentage of total rabies-labeled inputs in the PVH that co-stained with ISH probe. Both oxytocin$^+$ ($p < 0.001$, t test) and AVP$^+$ ($p = 0.02$) neurons showed a preference for sending input to VTA-GABA neurons. n = 6 (mice) for both probes in *DAT-Cre*, and n = 5 for both probes in *GAD2-Cre* mice.

(D–F) ISH in the LH for mRNAs encoding orexin (hypocretin) or NT, analogous to (A)–(C). (F) Both orexin neurons ($p = 0.0143$) and NT neurons ($p = 0.03$) showed a preference for VTA-DA neurons. n = 4 for all.

(G–I) ISH in the DR for genes encoding Tph2, GAD1/2, VGluT1/2/3, and TH in *DAT-Cre* mice. No TH$^+$/GFP$^+$ neurons were observed. (I) Serotonin ($p = 0.27$), GABA ($p = 0.97$), and glutamate ($p = 0.84$) neurons did not show a preference for VTA-DA or VTA-GABA neurons. n = 4 for all. The combined fraction exceeded 100% because a large fraction of neurons were both vGluT3$^+$ and Tph2$^+$.

All statistics were t tests. p values were obtained with Holm-Sidak correction for multiple comparisons where applicable. Scale, 100 μm. See Table S2 for related data.

peptides directly synapse onto VTA neurons. Co-labeling of RV*dG*-GFP with probes corresponding to oxytocin or AVP was observed when tracing inputs to both VTA-DA and VTA-GABA neurons (Figure 2B). For those GFP$^+$ PVH neurons that synapsed onto VTA-DA neurons, ~6% each were oxytocin$^+$ and AVP$^+$ (Figure 2C). These fractions increased to ~13% each for oxytocin$^+$ and AVP$^+$ neurons that synapsed onto VTA-GABA neurons (Figure 2C).

In the LH (Figure 2D), we used probes corresponding to the neuropeptides neurotensin (NT) and hypocretin (orexin), which also have been linked to reward-related behaviors (Korotkova et al., 2003; Kempadoo et al., 2013). NT$^+$ and orexin$^+$ neurons were labeled by RV*dG*-GFP in both *DAT-Cre* and *GAD2-Cre* mice, indicating that they synapse directly onto VTA-DA and VTA-GABA neurons (Figure 2E). Interestingly, both NT$^+$ and orexin$^+$ neurons exhibited a 2-fold preference for DA neurons (Figure 2F).

The DR contains heterogeneous neuronal populations that utilize different neurotransmitters, including serotonin, GABA, and glutamate (Weissbourd et al., 2014), and has recently been shown to send a reward signal to the VTA, largely through neurons that co-express both vGluT3 (a marker for a subset of glutamatergic neurons) and Tph2 (a serotonin neuron marker) (Liu et al., 2014; McDevitt et al., 2014). To determine the neurochemical identity of DR cells that synapse onto VTA-DA and VTA-GABA neurons, we used ISH probes designed to detect either (1) all three vesicular glutamate transporters (vGluT1/2/3), markers of excitatory glutamatergic neurons; (2) both glutamic acid decarboxylases

(GAD1/2), markers of inhibitory GABAergic neurons; or (3) Tph2. All three populations contributed a large fraction of DR input to both VTA-DA and VTA-GABA neurons with similar relative preferences (Figures 2G–2I).

Taken together, these results indicate that VTA neurons receive complex synaptic inputs from excitatory, inhibitory, and modulatory (serotonergic and peptidergic) neurons. These inputs synapse onto both VTA-DA and VTA-GABA neurons with some quantitative differences in their preferences.

TRIO and cTRIO Analyses Reveal Distinct Inputs onto VTA Neurons Based on Their Output

Previous studies have demonstrated considerable heterogeneity in the properties of VTA-DA neurons that correlates with the location to which VTA-DA neurons project (Lammel et al., 2008; Margolis et al., 2008). To investigate whether DA neurons projecting to different targets receive inputs from different brain areas, we utilized recently developed TRIO (for tracing the relationship between input and output) and cTRIO (for cell-type-specific TRIO) techniques (Schwarz et al., 2015). TRIO relies on the axonal uptake of *CAV-Cre*, a canine adenovirus vector expressing Cre recombinase that efficiently transduces axon terminals (Soudais et al., 2001). RV*dG*-mediated input tracing based on *CAV-Cre* injected at a projection site can reveal inputs to projection-defined VTA subpopulations (Figure S3A). cTRIO further refines input tracing to VTA-DA neurons that project to a specific output site by utilizing *CAV-FLEx^{loxP}-Flp* that expresses a Cre-dependent Flp recombinase in conjunction with AAVs expressing Flp-dependent TC and G in *DAT-Cre* mice (Figure 3A). Four major targets of DA neurons were selected for CAV injections: two subdivisions of the ventral striatum (lateral or medial nucleus accumbens [NAcLat and NAcMed]), medial prefrontal cortex (mPFC), and amygdala (Amy) (Figures 3B and S3B–S3E).

The starter cell locations in TRIO and cTRIO experiments were consistent with a topographic organization of VTA-DA neurons based on their projection targets (Lammel et al., 2008). Along the medial-lateral axis, starter cells for NAcLat-projecting neurons were more laterally distributed within the VTA compared to starter cells for NAcMed-projecting neurons, for example (Figures 3C, S3F, and S4). Quantification of VTA starter cells based on TH staining revealed that these four groups contained different fractions of DA neurons in the TRIO experiments, ranging from ~90% for NAcLat-projecting to <50% for mPFC- and Amy-projecting VTA neurons (Figure S3G), which is consistent with previous studies using conventional tracers (Swanson, 1982). By contrast, >90% of the starter cells for all four groups were TH+ in cTRIO experiments (Figure 3D), validating the neurochemical specificity of the cTRIO strategy.

Both TRIO and cTRIO analyses revealed quantitative differences in the inputs onto VTA neurons according to their outputs (Figures S3H and 3E); the variation in cTRIO experiments was smaller than for TRIO (Table S2), likely because starter cells were defined not only by projection but also cell type. We focus our discussion on cTRIO experiments because of the clear DA neuron identity. Notably, NAcLat-projecting VTA-DA neurons received proportionally more input from the anterior cortex, dorsal striatum, nucleus accumbens core (NAcCore) and lateral shell (NAcLatS), but less input from the DR, than the three other VTA-DA populations. In contrast, NAcMed-projecting DA neurons received preferential input from the NAc medial shell (NAcMedS) at the expense of the dorsal striatum (Figure 3E). These experiments demonstrate that VTA-DA neurons that project to different output sites receive biased input from selective regions, notably the DR and different striatal regions.

NAcMed- and NAcLat-Projecting DA Neurons Have Distinct Arborization Patterns

A striking finding from the TRIO and cTRIO analyses is that VTA-DA neurons that project to subdivisions of the ventral striatum (NAcMed versus NAcLat) receive highly biased inputs from different brain regions. This suggests that these projections originate from largely different populations of DA neurons. Indeed, individual VTA-DA neurons have been suggested to innervate one selective projection target based on lack of co-labeling of retrograde tracers injected into different VTA projection sites (Fallon, 1981; Swanson, 1982; Margolis et al., 2006a; Lammel et al., 2008). However, this methodology may not detect all axonal collateralizations because potential target regions can only be sampled one to three at a time. Additionally, incomplete coverage of the retrograde tracer within each sampled region may reduce the probability of detecting axon collateralization. To overcome these limitations, we employed an intersectional strategy to label VTA-DA neurons that project to a specific output target (Figure 4A) that allowed us to directly visualize axonal arbors of anatomically defined DA neurons, permitting a more comprehensive analysis of the axonal collateralization (or lack thereof) of specific DA neuron subpopulations.

We injected *CAV-FLEx^{loxP}-Flp* into the NAcLat or NAcMed of *DAT-Cre* mice and an AAV-expressing Flp-dependent membrane-tethered GFP (mGFP) into the VTA. This allowed examination of the axonal arborization pattern of NAcLat- or NAcMed-projecting VTA-DA neurons. Quantification of these axonal projections in ten brain regions revealed that the axon arbors of the NAcLat-projecting DA neurons largely avoided the NAc medial shell, while projecting more laterally and broadly in the striatum, including the dorsal striatum (Figures 4B and 4C; quantified in Figure 4D). By contrast, axonal arbors of NAcMed-projecting VTA-DA neurons were highly enriched in the NAc medial shell (Figure 4B, quantified in Figure 4D) but largely avoided the NAc lateral shell. In total, NAcLat-projecting DA neurons had 3-fold broader arborizations in the striatum than NAcMed-projecting DA neurons (Figure 4E). Very few axonal arbors were observed in the mPFC or central amygdala from either condition. Interestingly, while the axonal arbors of NAcLat-projecting DA neurons were largely confined to the striatum, NAcMed-projecting DA neurons sent significant collaterals outside the striatum, including the septum and ventral pallidum, indicating that this DA subpopulation is capable of simultaneously influencing neural activity in multiple brain regions.

Electrophysiological Examination of Synaptic Connections Predicted by cTRIO

cTRIO analysis of the input-output relationships of VTA-DA neurons revealed several previously unrecognized connectivity patterns. To determine whether they represent functional connections, we performed ex vivo electrophysiological assays, in

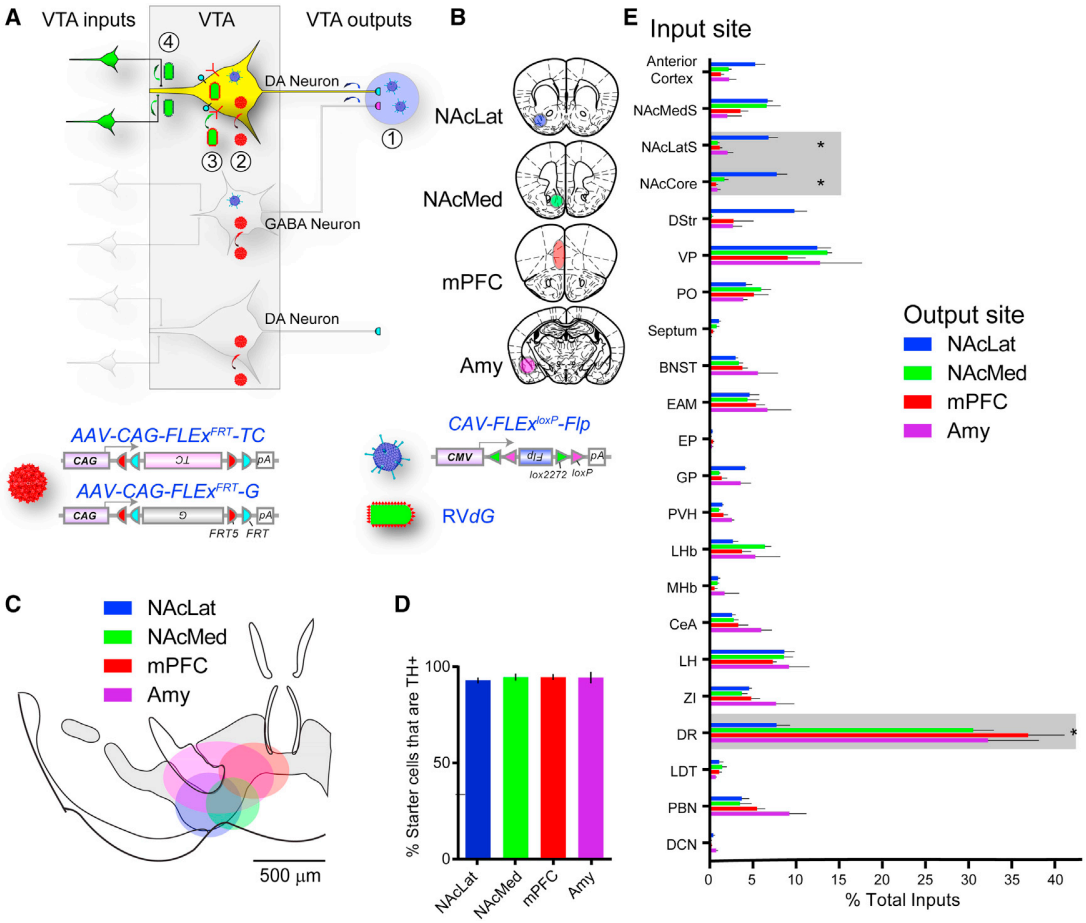

Figure 3. cTRIO Analysis of the Input-Output Relationships of VTA-DA Neurons

(A and B) Schematic of cTRIO experiments. (1) *CAV-FLEx^{loxP}-Flp* was injected into one of four output sites (coronal schematics in B). (2) On the same day, AAVs that express Flp-dependent TC and G were injected into the VTA. (3) Two weeks later, RV*d*G was injected into the VTA. (4) Five days later, histological analyses were performed.

(C) Average starter cell distributions in the VTA for four cTRIO conditions. The center of each oval represents the center of mass of starter cells, and the horizontal and vertical radii of the oval represent one SD of starter cells in the medial-lateral and dorsal-ventral axes, respectively. See Figure S4 for more details.

(D) Percentage of starter cells that co-labeled with TH for each cTRIO condition.

(E) Whole-brain input data to each of the VTA neuronal populations defined by cTRIO (n = 4 for each condition). Percentage of total inputs is plotted on the x axis, and brain region is plotted on the y axis. Brain regions with significant differences ($p < 0.05$, one-way ANOVA for each brain region, with Holm-Sidak correction for 22 one-way ANOVAs) are highlighted in gray. Asterisk (*) shows NAcLatS, NAcCore, and DR send significantly different fractional input to NAcLat-projecting VTA-DA neurons compared to NAcMed, mPFC, and Amy-projecting VTA-DA neurons ($p < 0.05$, post hoc pairwise comparisons with Holm-Sidak corrections for 6 comparisons). Because NAcLat-projecting VTA-DA neurons produce the most inputs (Table S1), the input distribution from NAcLat-based cTRIO resembles Figure 1P the most.

See Figure 1 for abbreviation of anatomical regions and Figures S2, S3, and S4 and Tables S1, S2, and S3 for related data.

which we optically activated individual VTA inputs expressing channelrhodopsin-2 (ChR2) while recording from identified DA neurons projecting to specific targets labeled with retrobeads (Lammel et al., 2012).

Previous work suggested that lateral habenula (LHb) neurons do not make synaptic connections onto VTA-DA neurons projecting to the NAcLat (Lammel et al., 2012), whereas cTRIO analysis suggests that LHb inputs comprised ~3% of all inputs to this population. To investigate this discrepancy, we injected an AAV-expressing ChR2 into the LHb and red retrobeads into the NAcLat of transgenic mice in which DA neurons were GFP$^+$ (Figure 5A). Whole-cell recordings were made from acute slices containing VTA neurons that were both green (DA$^+$) and red (NAcLat projecting). Light-evoked synaptic responses were observed in 2 of 26 recorded neurons (Figures 5B–5D), which were blocked by the AMPA receptor antagonist CNQX. These observations are consistent both with previous observations that the LHb input to NAcLat-projecting VTA-DA neurons is sparse (zero of four cells; Lammel et al., 2012) and with our cTRIO results showing that such a connection exists. The location of responding neurons may explain why previous electrophysiology studies may have missed this connection, as the responding cells were

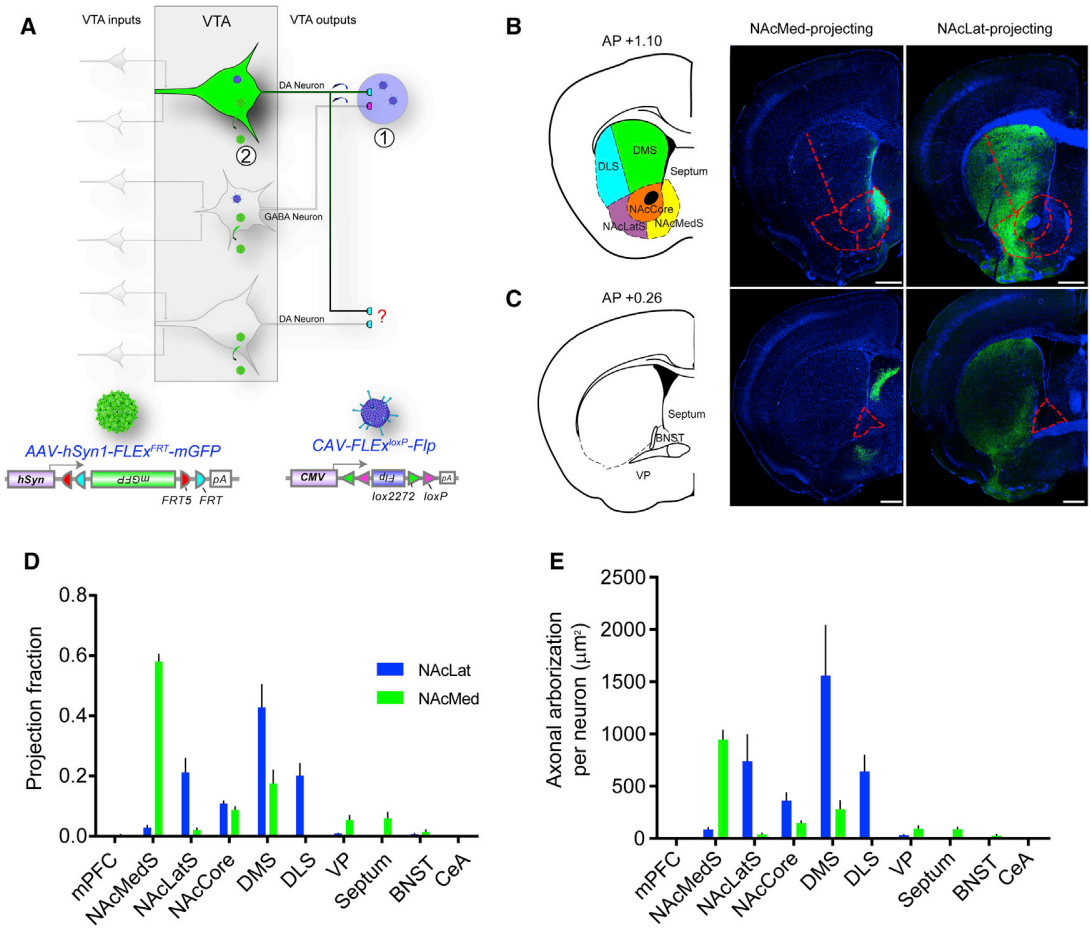

Figure 4. Axonal Arborization Analysis of NAcLat- and NAcMed-Projecting VTA-DA Neurons

(A) Schematic of experimental setup. (1) *CAV-FLEx^{loxP}-Flp* was injected into either the NAcLat or NAcMed. (2) On the same day, an AAV expressing Flp-dependent membrane-GFP was injected into the VTA. Brains were harvested 2 months later.

(B) Representative coronal sections showing axonal projections of NAcMed-projecting (middle) and NAcLat-projecting (right) VTA-DA neurons in the striatum, along with an atlas schematic (left). Dotted lines outline subdivisions of the striatum. DLS, dorsolateral striatum; DMS, dorsomedial striatum.

(C) Same as in (B) except more posterior coronal sections are shown. Dotted lines outline the BNST.

(D) Proportion of total arborization of NAcMed- and NAcLat-projecting VTA-DA neurons across ten brain regions. An average of 349 ± 80 VTA-DA neurons were labeled by targeting the NAcMed (n = 5) and 366 ± 106 neurons by the NAcLat (n = 4).

(E) NAcLat-projecting DA neurons showed a broader arborization than NAcMed-projecting DA neurons, as evidenced by a greater area covered by labeled axonal arbors. Scale, 500 μm.

located more ventrally (Figure 5B) than expected for NAcLat-projecting DA neurons (Lammel et al., 2008). This example also illustrates that rabies-based trans-synaptic techniques have the sensitivity to uncover relatively rare connections that could be missed using other techniques.

Another surprising cTRIO result is that the anterior cortex, including the mPFC, makes monosynaptic connections onto NAc-projecting DA neurons (Figure 3E). Previous electron microscopy studies using classical tracers suggested that mPFC inputs to the VTA synapse onto mPFC-projecting but not onto NAc-projecting DA neurons (Carr and Sesack, 2000). To investigate this discrepancy, we performed similar electrophysiological recordings to those just described but injected the AAV-expressing ChR2 into the mPFC. 5 of 37 NAcLat-projecting VTA-DA neurons showed a time-locked response to photostimulation (Figures 5B–5D), functionally validating a pathway identified by cTRIO. As our input tracing data demonstrated that anterior cortical input to VTA-DA neurons also arose from other frontal cortical regions besides the mPFC (Figure S5), in separate experiments we injected the AAV-expressing ChR2 into broader anterior cortical regions, including the insular and orbitofrontal cortices in addition to the mPFC. In these mice, 19 of 36 NAcLat-projecting VTA-DA neurons showed a time-locked response to photostimulation that was blocked by CNQX. These connections also displayed a higher mean EPSC amplitude (28.4 ± 7.7 pA for anterior cortex versus 14.9 ± 3.0 pA for mPFC, Figure 5E), likely due to more anterior cortical cells expressing ChR2. Thus, our data suggest that signals arising

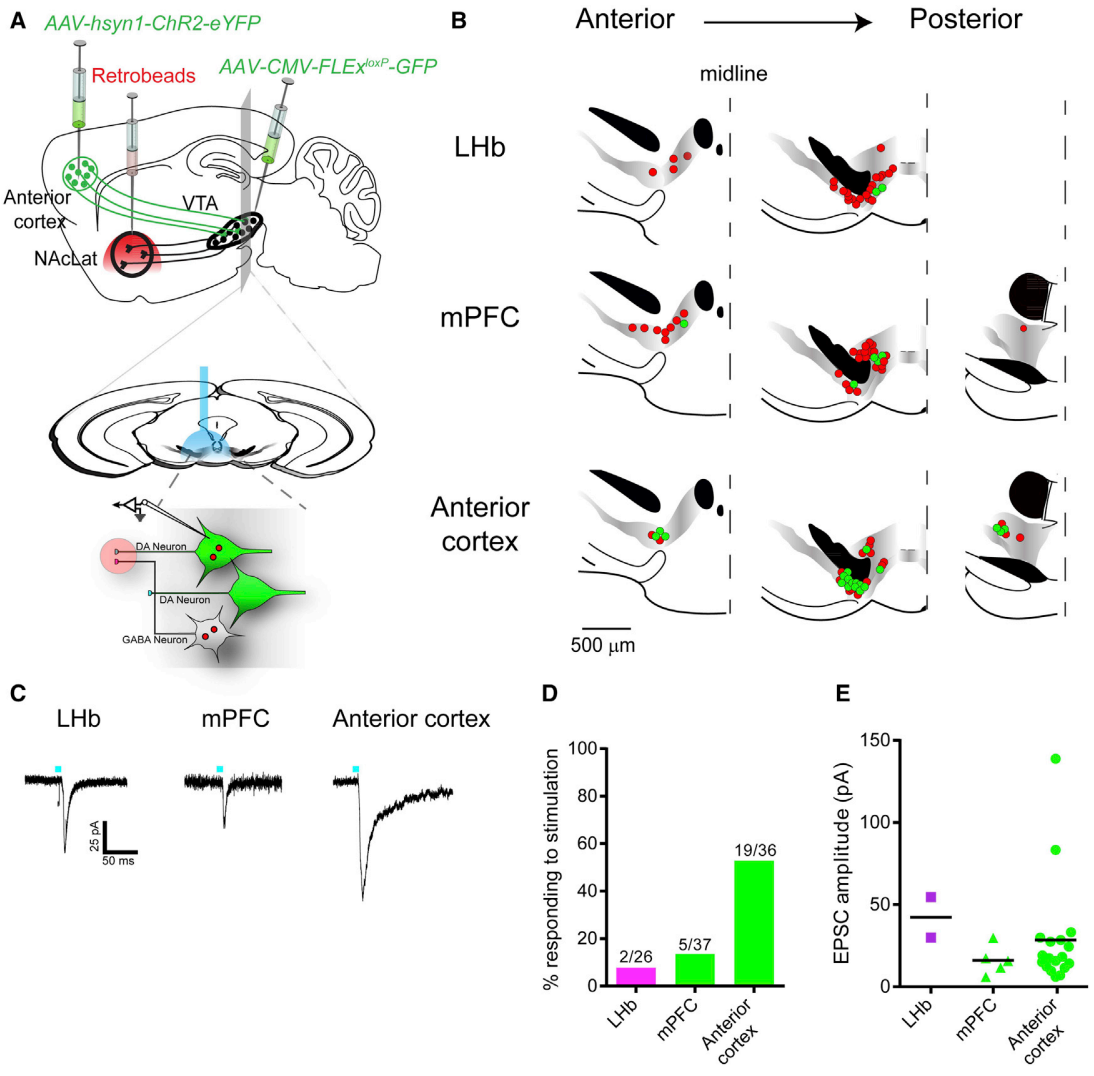

Figure 5. Electrophysiological Validation of New Pathways Identified Using cTRIO

(A) Schematic of experimental setup. An AAV expressing ChR2-eYFP was injected into the lateral habenula (LHb), mPFC, or anterior cortex (depicted); red retrobeads were injected into the NAcLat; and *AAV-CMV-FLEx^{loxP}-GFP* was injected into the VTA of a *DAT-Cre* mouse. Two months later, whole-cell recordings were conducted from GFP^{+} retrobead^{+} neurons in acute VTA slices while photostimulating ChR2-expressing axons and terminals.

(B) Map of responding (green) and non-responding (red) cells to photostimulation.

(C) Sample EPSCs from identified VTA-DA neurons receiving inputs from the LHb, mPFC, or anterior cortex.

(D) Quantification of connectivity from each input site.

(E) Average EPSC amplitudes from responding cells at –60 mV in each experiment. Colored shapes and black bars indicate individual values and the means, respectively.

See Figure S5 for related data.

from the anterior cortex are capable of influencing neural activity in a large proportion of NAcLat-projecting VTA-DA neurons.

The Anterior Cortex→VTA-DA→NAcLat Circuit Is Reinforcing

We next asked what role the anterior cortex→VTA-DA→NAcLat circuit could play in behavior. As the anterior cortex provided excitatory input onto NAcLat-projecting VTA-DA neurons in our slice recordings, we hypothesized that activation of anterior cortical inputs to the VTA in vivo would lead to DA release in the NAcLat, which would be reinforcing. To test this hypothesis, we injected mice with an AAV expressing either ChR2-eYFP (n = 7) or eYFP alone (n = 8) into the anterior cortex (including the mPFC, insular, and orbitofrontal cortices) and implanted optical fibers targeted just dorsal to the VTA (Figures 6A, 6B, and S6). After waiting 2 to 3 months, mice were subjected to an intracranial self-stimulation (ICSS) procedure during which they were allowed to respond freely at 5 adjacent nosepoke ports for

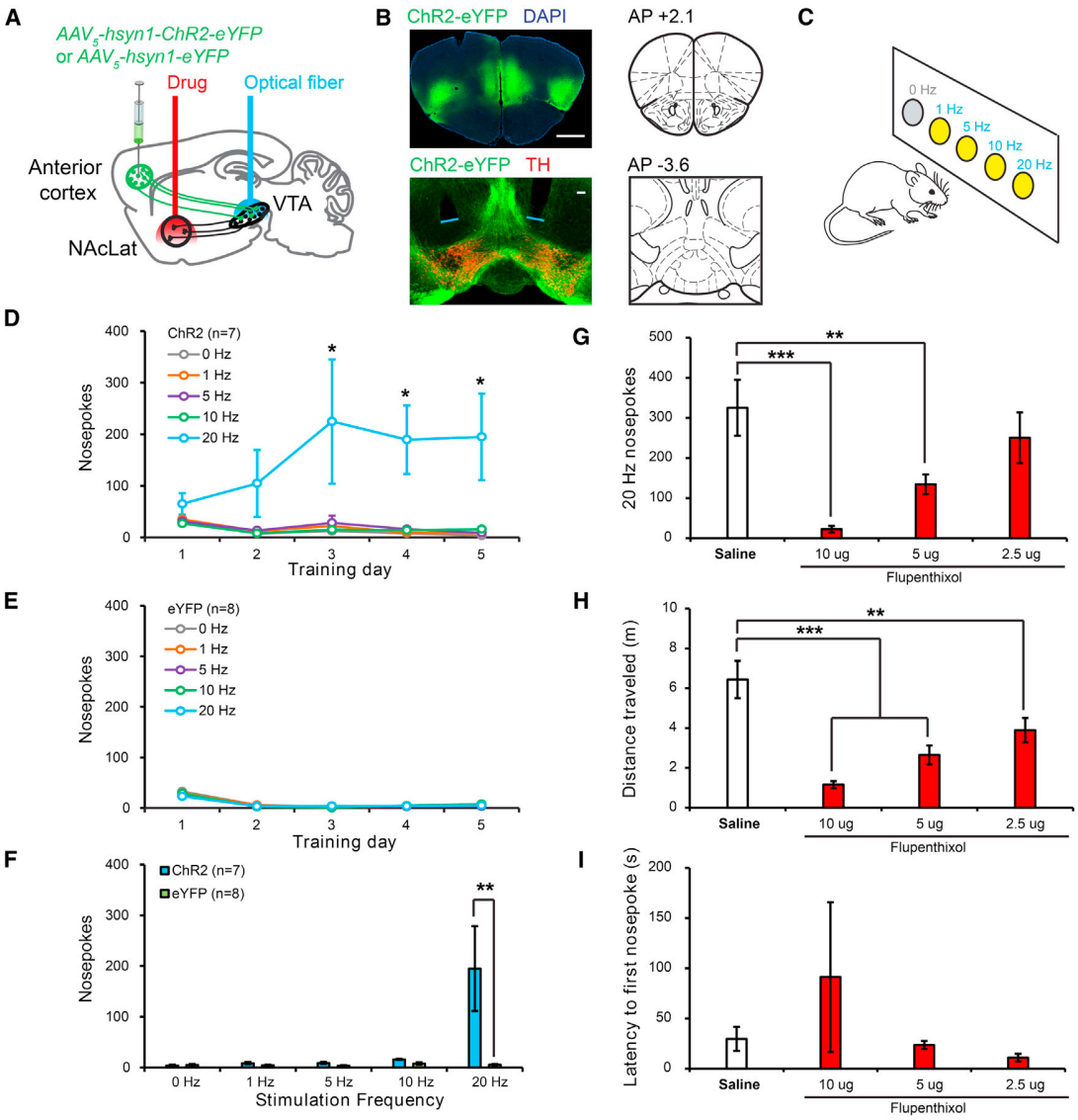

Figure 6. Behavioral Function of the Anterior Cortex→VTA-DA→NAcLat Circuit

(A) Schematic of experimental setup. An AAV expressing either ChR2-eYFP or eYFP was injected into the anterior cortex (medial and lateral sites), and optical fibers were implanted above the VTA so that anterior cortex axon terminals innervating the VTA could be optically stimulated. A guide cannula was also implanted targeting the NAcLat in all mice for drug delivery in some experiments. All manipulations were bilateral.

(B) Top, ChR2-eYFP expression following virus injection into the anterior cortex. Scale, 1 mm. Bottom, ChR2-eYFP-expressing axon terminals in the VTA of the same mouse. Blue lines indicate optical fiber tips. Scale, 100 μm.

(C) Schematic of ICSS task. Mice were allowed to respond freely at 5 nosepoke ports for 1 hr per day over 5 training days. A response at 4 ports resulted in the delivery of a 2 s train of light pulses at varying frequencies (1, 5, 10, and 20 Hz); an LED in the back of the port was concurrently illuminated to serve as a visual cue indicating ongoing stimulation. Responses at a fifth control port (0 Hz) had no consequence. For the first training session, all nosepokes were baited to facilitate initial investigation.

(D) Mice expressing ChR2-eYFP (n = 7) developed a strong preference for the 20 Hz port as compared to the 0 Hz control port (one-way Friedman repeated-measures ANOVA on ranks, main effect of nosepoke type $p < 0.006$ on days 3–5; 20 Hz versus 0 Hz $p < 0.05$, Tukey post hoc tests).

(E) Mice expressing eYFP (n = 8) responded at similarly low levels at all nosepoke ports ($p > 0.351$, days 1–5).

(F) On training day 5, ChR2-eYFP mice made significantly more nosepokes at the 20 Hz port than eYFP mice (Mann-Whitney Rank-Sum test with Bonferroni correction, $p = 0.005$), indicating that optical activation of the anterior cortex-VTA projection is reinforcing.

(G–I) Infusion of the non-selective dopamine receptor antagonist flupenthixol into the NAcLat dose-dependently decreased responding for 20 Hz stimulation of anterior cortex→VTA projections in ChR2-eYFP-expressing mice (n = 5) (G; one-way repeated-measures ANOVA, main effect of drug $p < 0.001$; 10 μg and 5 μg flupenthixol versus saline vehicle; $p < 0.001$ and $p = 0.01$, respectively, Holm-Sidak post hoc tests). Doses indicate amount of drug delivered per hemisphere in 0.25 μl saline. While locomotion was concurrently decreased by flupenthixol (H; one-way repeated-measures ANOVA, main effect of drug $p < 0.001$; 10 μg,

(legend continued on next page)

photostimulation. Responses at 4 ports resulted in photostimulation of anterior cortex→VTA projections at varying stimulation frequencies (1, 5, 10, or 20 Hz) for 2 s; responses at a fifth control port did not result in any stimulation (Figure 6C). ChR2-eYFP-expressing mice developed a strong preference for the 20 Hz port over successive training days, making significantly more responses at this port than at the control port that did not produce stimulation (Figure 6D). In contrast, eYFP-expressing control mice did not show this preference (Figures 6E and 6F).

To determine whether the reinforcing effects of anterior cortex→VTA projection stimulation required DA release in the NAcLat, we combined site-specific pharmacology with our optogenetic manipulation. In a subset of high-responding ChR2-eYFP-expressing mice (n = 5), we infused varying doses of flupenthixol, a non-selective DA receptor antagonist, or saline vehicle, into the NAcLat via previously implanted cannulae targeting this area (see Supplemental Experimental Procedures; Figures 6A and S6). Flupenthixol infusion into the NAcLat prior to ICSS behavioral sessions resulted in a dose-dependent decrease in responding for 20 Hz stimulation of anterior cortex→VTA projections (Figure 6G), which is consistent with our hypothesis that optically evoked DA release in NAcLat was a critical mediator of the ICSS behavior we observed. Flupenthixol infusion also reduced locomotion during ICSS sessions (Figure 6H). However, the latency to initiate response at the 20 Hz nosepoke port was unaffected (Figure 6I), indicating that mice were physically capable of making nosepoke responses under the influence of flupenthixol. Importantly, because behavioral sessions did not begin until >10 min after drug infusions were complete, DA receptors in the NAcLat were likely to be fully blocked at the beginning of the session when latency measurements were recorded.

Taken together, these data suggest that the anterior cortex makes direct, excitatory synaptic connections onto VTA-DA neurons projecting to the NAcLat and that activation of this circuit is reinforcing.

DISCUSSION

We have utilized rabies-mediated trans-synaptic tracing and TRIO/cTRIO to dissect the complex circuits in which midbrain VTA-DA neurons participate. Our unbiased anatomical mapping revealed the global input-output architecture of the majority of VTA-DA neurons. We validated two previously unknown circuits with electrophysiology and identified a behavioral function of one of the new circuits. Below, we discuss the technical and conceptual implications of these findings.

Technical Considerations

Recent trans-synaptic tracing techniques have permitted systematic, high-resolution analyses of inputs based on the location, genetic identity (cell type), or axonal projection of starter cells (Callaway and Luo, 2015). cTRIO simultaneously leverages all of these targeting strategies, thereby allowing access to more specific starter cell populations for dissecting complex circuits, such as those involving VTA-DA neurons. A previous method of labeling inputs based on outputs of VTA-DA neurons relied on RV*dG* injection directly into an output site and trans-complementing the virus in VTA-DA neurons by expressing G under the control of *TH-Cre* (Lammel et al., 2012). A caveat of this method is that if RV*dG* spread among DA neurons, input-output specificity would be compromised, as all *TH-Cre*-expressing neurons would be competent to initiate trans-synaptic tracing. As TRIO and cTRIO limit TC and G expression only to neurons projecting directly to the target site, the input-output relationship is preserved even if VTA-DA neurons are locally connected. In addition, TRIO and cTRIO produced about 10-fold more efficient labeling than the previous method (Lammel et al., 2012), thus identifying more comprehensive monosynaptic inputs to projection-based VTA-DA subpopulations.

The electrophysiological validations of new connections identified in our cTRIO experiments highlight the sensitivity of rabies-mediated trans-synaptic tracing techniques. Although previous electrophysiological (Lammel et al., 2012) and electron microscopy studies (Carr and Sesack, 2000) failed to identify LHb→VTA-DA→NAcLat or mPFC→VTA-DA→NAcLat circuits, their presence in our cTRIO experiments motivated a further examination. Our observations support the hypothesis that the LHb sends a weak input to the NAcLat-projecting VTA-DA neurons. We also identified and validated direct synaptic connections from the mPFC onto VTA-DA neurons projecting to the NAc.

Although electron microscopy and slice electrophysiology are powerful methods for studying circuit architecture and function, they are less suited for large-scale connectivity analyses. TRIO/cTRIO provide a global "scaffold" to identify input-output architecture of a region and/or cell types of interest. The properties and function of the circuits can be further investigated using complementary methods such as electrophysiology and optogenetics, as exemplified in our study. These combined approaches can be applied to many other cell types and circuits in the mammalian brain.

Architecture of VTA-DA Circuitry

Our whole-brain trans-synaptic tracing experiments from VTA-DA and VTA-GABA neurons have extended previous findings (Watabe-Uchida et al., 2012). We observed that both types of neurons receive inputs from a wide variety of brain regions, with overall similar distributions (Figure 1). This is reminiscent of our recent input-tracing study in the DR, where serotonin and GABA neurons receive qualitatively similar input from diverse brain regions (Weissbourd et al., 2014). This common feature could be used for input to VTA or DR GABA neurons to serve as feed-forward inhibition to regulate the activity of DA or serotonin neurons. As is the case for DR-serotonin and -GABA neurons, VTA-DA and -GABA neurons receive diverse direct input from excitatory, inhibitory, and modulatory neurons,

5 μg and 2.5 μg flupenthixol versus saline vehicle; $p < 0.001$, $p < 0.001$, and $p = 0.003$, respectively, Holm-Sidak post hoc tests), the latency to make the first response was unaffected (I; $p = 0.482$), indicating that mice were physically capable of performing nosepoke responses during behavioral sessions where flupenthixol was administered.
See Figure S6 for related data.

including prominent direct input from DR serotonin and GABA neurons (Figure 2), highlighting the complex regulation of these neuromodulatory systems and their rich interactions.

In addition to the complex input patterns, VTA-DA neurons project to diverse output sites that appear to correlate with their intrinsic properties, cell body location, and, in one specific example, input preference (Lammel et al., 2008, 2011, 2012). Our TRIO/cTRIO analyses have provided a comprehensive overview of the input-output relationships of multiple subtypes of VTA-DA neurons projecting to four principal output sites: the nucleus accumbens (NAcMed and NAcLat), medial prefrontal cortex, and amygdala. Our data confirmed a correlation between VTA output sites and the location of the cell soma within the VTA (Figure S4). At the same time, these data have produced a more nuanced picture of the input-output relationships of this complex structure than the discrete pathways suggested by a previous study (Lammel et al., 2012), likely reflecting the sensitivity of the TRIO techniques (see above). Qualitatively, VTA-DA neurons projecting to all output sites receive input from all 22 brain regions examined in this study. Quantitatively, however, input patterns can be highly biased depending on the output sites (Figures 3 and S3). NAcLat-projecting VTA-DA neurons have the most distinct input patterns compared with the three other groups of VTA-DA neurons examined in this study. Furthermore, our axonal arborization analysis (Figure 4) demonstrates that NAcLat-projecting VTA-DA neurons have little overlap with NAcMed-projecting VTA-DA neurons in their striatal target regions and that NAcMed-projecting VTA-DA neurons have previously unknown extra-striatal collateralization. Thus, our data support a biased input/discrete output architecture for VTA-DA circuitry. A similar input-output architecture also applies to SNc-DA circuitry (Lerner et al., 2015 [in this issue of *Cell*]).

As the major output site of VTA-DA neurons and a crucial structure implicated in reward processing and drug addiction, the nucleus accumbens has been intensively studied. However, NAc-projecting DA neurons have been considered a homogeneous population. Our data demonstrate that NAcMed- and NAcLat-projecting VTA-DA neurons represent two discrete populations with distinct targets and receive differential inputs. NAcLat-projecting VTA-DA neurons preferentially receive input from the anterior cortex and striatal regions, whereas NAcMed-projecting VTA-DA neurons preferentially receive input from the dorsal raphe (Figure 3E). Together with the differential gene expression and firing patterns, these observations strongly suggest that these DA neuron subpopulations are integrated into different circuits and serve distinct biological functions. These findings highlight the importance of differentiating DA neuron subpopulations and NAc sub-regions where possible in future studies.

The observations of discrete outputs and specific input-output relationships for VTA-DA neurons contrast with the architecture of locus coeruleus norepinephrine (LC-NE) circuits. LC-NE neurons received similar inputs regardless of where they project, and projection-defined subpopulations of LC-NE neurons also project to all brain regions examined (Schwarz et al., 2015). Although these catecholamine circuits have sometimes been treated as complementary systems, with the DA neurons projecting to the striatum and NE neurons elsewhere, their input-output structures are markedly different. The NE circuit architecture is consistent with a role to "broadcast" a general message throughout the brain, which may be optimal for coordinating brain states such as sleep and arousal. The DA system is better suited for sending discrete signals. For example, subpopulations of VTA-DA neurons have previously been found to differentially encode reward and aversion in mice (Lammel et al., 2012) and non-human primates (Matsumoto and Hikosaka, 2009). Indeed, the circuit architecture of using parallel channels to encode discrete information may be evolutionarily conserved; recent studies have identified unique populations of *Drosophila* DA neurons carrying appetitive or aversive signals that project to discrete zones of the mushroom body, an insect center for learning and memory (Aso et al., 2014).

A Top-Down Reinforcement Signal

In this study, we identified a behavioral function of a previously unappreciated connection from the anterior cortex to NAcLat-projecting VTA-DA neurons. Although prior work demonstrated that altering activity in the PFC changes DA levels in the striatum (e.g., Karreman and Moghaddam, 1996), other data suggested that a direct mPFC→VTA-DA→NAcLat circuit did not exist (Carr and Sesack, 2000). Our cTRIO studies revealed a monosynaptic connection from the anterior cortex to NAcLat-projecting DA neurons, a finding that we confirmed with ex vivo electrophysiological recordings from identified NAcLat-projecting VTA-DA neurons. Using optogenetics and behavioral pharmacology, we identified a functional role for this circuit in mediating positive reinforcement. Thus, our data suggest that frontal cortical regions are capable of exerting top-down control of midbrain neurons that contribute to motivated behaviors via DA release in the NAc, bypassing other intermediary regions such as the LDT and striatum to directly engage DA neurons and exert executive control over a powerful neuromodulatory system.

In summary, our data add to a growing body of evidence in favor of a model wherein functionally distinct midbrain DA neuron subtypes encode different signals and participate in largely separate yet interconnected circuits through their biased input and discrete output pathways. However, much remains to be understood. For example, investigating the circuit properties of NAc inputs onto both DA and GABA neurons (feedback and feed-forward inhibition) and defining the message encoded in the firing patterns of each of these DA neuron subpopulations in response to various natural stimuli will be necessary to understand the normal and pathophysiological functions of these important circuits.

EXPERIMENTAL PROCEDURES

Mice and Viral Procedures

DAT-Cre (Bäckman et al., 2006), tdTomato Cre reporter *Ai14* (Madisen et al., 2010), and C57Bl/6 mice were obtained from the Jackson Laboratories, and *GAD2-Cre* mice (Taniguchi et al., 2011) were obtained from Josh Huang. Mice were housed on a 12 hr light/dark cycle with food and water ad libitum. Viral vectors were prepared as previously described (Schwarz et al., 2015). Detailed procedures for rabies tracing, TRIO, cTRIO, and axonal arborization are described in the Supplemental Experimental Procedures. All procedures followed animal care and biosafety guidelines approved by Stanford University's Administrative Panel on Laboratory Animal Care and Administrative Panel of Biosafety.

Electrophysiology

Six-week-old *DAT-Cre* mice were injected with *AAV_1-CMV-FLEx-GFP* into the VTA, rhodamine-conjugated retrobeads into the NAcLat, and *AAV_{DJ}-hsyn1-ChR2(H134R)-eYFP* into the LHb, mPFC, or anterior cortex. 8 weeks later, recordings were done as previously described (Lammel et al., 2011). Excitatory postsynaptic currents (EPSCs) were recorded in whole-cell voltage clamp; series resistance and input resistance were monitored on-line with a 4 mV hyperpolarizing step (50 ms). Neurons were voltage clamped at –60 mV to record AMPAR EPSCs. For drug application, CNQX (10 μM) was added to the ACSF. Connections were defined as neurons that exhibited an average current (over 5 sweeps) of ≥10 pA recorded either at –60 mV or +40 mV.

Behavior

AAV_5-hsyn1-eYFP or *AAV_5-hsyn1-ChR2(H134R)-eYFP* (0.5 μl) was infused bilaterally into the anterior cortex of C57Bl/6 mice. Optical fibers were implanted dorsal to the VTA, and cannulae were implanted targeting the NAcLat. More than 8 weeks following virus infusions, ChR2-eYFP mice and eYFP controls were given 5 daily ICSS training sessions during which they could respond at 5 nosepoke ports. A response at each port produced 2 s of 473 nm light, pulsed at a particular frequency (20, 10, 5, 1, or 0 Hz). Following ICSS training, a subset of high-responding ChR2-eYFP mice was used for drug infusion studies. These mice received bilateral 0.25 μl infusions of either flupenthixol (F114, Sigma, dissolved in saline) or saline vehicle through the implanted guide cannula 10 min prior to ICSS sessions.

Statistical Analysis

Results of all statistical analyses for tracing experiments are provided in Table S2. For each input brain region, paired t tests were used for input tracing and ISH experiments, and one-way ANOVAs were used for TRIO and cTRIO data, with correction for multiple comparisons. (We did not use two-way ANOVA because the data from different brain regions did not meet the equal variance assumption.) For starter cell distributions, t tests were used with corrections for multiple comparisons. Behavioral data were analyzed with parametric or non-parametric one-way repeated-measures ANOVAs followed by Holm-Sidak or Tukey post hoc tests.

SUPPLEMENTAL INFORMATION

Supplemental Information includes Supplemental Experimental Procedures, six figures, and three tables and can be found with this article online at http://dx.doi.org/10.1016/j.cell.2015.07.015.

AUTHOR CONTRIBUTIONS

K.T.B., R.C.M., and L.L. designed the study. K.T.B. performed most of the experiments and data analysis. E.E.S. designed and performed the behavioral experiments and data analysis. K.E.D. and S.X. provided technical assistance. K.M., L.S., and E.J.K. contributed to TRIO and cTRIO development and characterization. X.J.G. helped with data analysis. K.T.B. and L.L. wrote the paper with substantial contributions from E.E.S. and R.C.M.

ACKNOWLEDGMENTS

We thank P. Temkin for reagents; S. Lammel and M. Taylor for technical assistance and helpful discussions; T. Lerner, B. Weissbourd, and T. Mosca for advice and critiques on the manuscript; and K. Deissorth for coordinating publications. This work was supported by an NIH grant (TR01MH099647) and a Hughes Collaborative Innovation Award to L.L., an NRSA Postdoctoral Fellowship (1F32DA038913-01) to K.T.B., and a grant from the Simons Foundation Autism Research Initiative and the NIMH Silvio Conte Center at Stanford (P50 MH086403) to R.C.M.

Received: May 11, 2015
Revised: July 2, 2015
Accepted: July 8, 2015
Published: July 30, 2015

REFERENCES

Aso, Y., Hattori, D., Yu, Y., Johnston, R.M., Iyer, N.A., Ngo, T.T., Dionne, H., Abbott, L.F., Axel, R., Tanimoto, H., and Rubin, G.M. (2014). The neuronal architecture of the mushroom body provides a logic for associative learning. eLife *3*, e04577.

Bäckman, C.M., Malik, N., Zhang, Y., Shan, L., Grinberg, A., Hoffer, B.J., Westphal, H., and Tomac, A.C. (2006). Characterization of a mouse strain expressing Cre recombinase from the 3′ untranslated region of the dopamine transporter locus. Genesis *44*, 383–390.

Beckstead, R.M., Domesick, V.B., and Nauta, W.J. (1979). Efferent connections of the substantia nigra and ventral tegmental area in the rat. Brain Res. *175*, 191–217.

Brischoux, F., Chakraborty, S., Brierley, D.I., and Ungless, M.A. (2009). Phasic excitation of dopamine neurons in ventral VTA by noxious stimuli. Proc. Natl. Acad. Sci. USA *106*, 4894–4899.

Bromberg-Martin, E.S., Matsumoto, M., and Hikosaka, O. (2010). Dopamine in motivational control: rewarding, aversive, and alerting. Neuron *68*, 815–834.

Callaway, E.M., and Luo, L. (2015). Monosynaptic circuit tracing with glycoprotein-deleted rabies viruses. J. Neurosci. *35*, 8979–8985.

Carr, D.B., and Sesack, S.R. (2000). Projections from the rat prefrontal cortex to the ventral tegmental area: target specificity in the synaptic associations with mesoaccumbens and mesocortical neurons. J. Neurosci. *20*, 3864–3873.

Cohen, J.Y., Haesler, S., Vong, L., Lowell, B.B., and Uchida, N. (2012). Neuron-type-specific signals for reward and punishment in the ventral tegmental area. Nature *482*, 85–88.

Fallon, J.H. (1981). Collateralization of monoamine neurons: mesotelencephalic dopamine projections to caudate, septum, and frontal cortex. J. Neurosci. *1*, 1361–1368.

Fields, H.L., Hjelmstad, G.O., Margolis, E.B., and Nicola, S.M. (2007). Ventral tegmental area neurons in learned appetitive behavior and positive reinforcement. Annu. Rev. Neurosci. *30*, 289–316.

Jin, X., and Costa, R.M. (2010). Start/stop signals emerge in nigrostriatal circuits during sequence learning. Nature *466*, 457–462.

Karreman, M., and Moghaddam, B. (1996). The prefrontal cortex regulates the basal release of dopamine in the limbic striatum: an effect mediated by ventral tegmental area. J. Neurochem. *66*, 589–598.

Kempadoo, K.A., Tourino, C., Cho, S.L., Magnani, F., Leinninger, G.M., Stuber, G.D., Zhang, F., Myers, M.G., Deisseroth, K., de Lecea, L., and Bonci, A. (2013). Hypothalamic neurotensin projections promote reward by enhancing glutamate transmission in the VTA. J. Neurosci. *33*, 7618–7626.

Korotkova, T.M., Sergeeva, O.A., Eriksson, K.S., Haas, H.L., and Brown, R.E. (2003). Excitation of ventral tegmental area dopaminergic and nondopaminergic neurons by orexins/hypocretins. J. Neurosci. *23*, 7–11.

Lammel, S., Hetzel, A., Häckel, O., Jones, I., Liss, B., and Roeper, J. (2008). Unique properties of mesoprefrontal neurons within a dual mesocorticolimbic dopamine system. Neuron *57*, 760–773.

Lammel, S., Ion, D.I., Roeper, J., and Malenka, R.C. (2011). Projection-specific modulation of dopamine neuron synapses by aversive and rewarding stimuli. Neuron *70*, 855–862.

Lammel, S., Lim, B.K., Ran, C., Huang, K.W., Betley, M.J., Tye, K.M., Deisseroth, K., and Malenka, R.C. (2012). Input-specific control of reward and aversion in the ventral tegmental area. Nature *491*, 212–217.

Lammel, S., Steinberg, E.E., Földy, C., Wall, N.R., Beier, K., Luo, L., and Malenka, R.C. (2015). Diversity of transgenic mouse models for selective targeting of midbrain dopamine neurons. Neuron *85*, 429–438.

Lerner, T.N., Shilyansky, C., Davidson, T.J., Evans, K.E., Beier, K.T., Zalocusky, K.A., Crow, A.K., Malenka, R.C., Luo, L., Tomer, R., and Deisseroth, K. (2015). Intact-brain analyses reveal distinct information carried by SNc dopamine subcircuits. Cell *162*, this issue, 635–647.

Liu, Z., Zhou, J., Li, Y., Hu, F., Lu, Y., Ma, M., Feng, Q., Zhang, J.E., Wang, D., Zeng, J., et al. (2014). Dorsal raphe neurons signal reward through 5-HT and glutamate. Neuron *81*, 1360–1374.

Madisen, L., Zwingman, T.A., Sunkin, S.M., Oh, S.W., Zariwala, H.A., Gu, H., Ng, L.L., Palmiter, R.D., Hawrylycz, M.J., Jones, A.R., et al. (2010). A robust and high-throughput Cre reporting and characterization system for the whole mouse brain. Nat. Neurosci. *13*, 133–140.

Margolis, E.B., Lock, H., Chefer, V.I., Shippenberg, T.S., Hjelmstad, G.O., and Fields, H.L. (2006a). κ opioids selectively control dopaminergic neurons projecting to the prefrontal cortex. Proc. Natl. Acad. Sci. USA *103*, 2938–2942.

Margolis, E.B., Lock, H., Hjelmstad, G.O., and Fields, H.L. (2006b). The ventral tegmental area revisited: is there an electrophysiological marker for dopaminergic neurons? J. Physiol. *577*, 907–924.

Margolis, E.B., Mitchell, J.M., Ishikawa, J., Hjelmstad, G.O., and Fields, H.L. (2008). Midbrain dopamine neurons: projection target determines action potential duration and dopamine D(2) receptor inhibition. J. Neurosci. *28*, 8908–8913.

Marinelli, M., and McCutcheon, J.E. (2014). Heterogeneity of dopamine neuron activity across traits and states. Neuroscience *282C*, 176–197.

Matsumoto, M., and Hikosaka, O. (2009). Two types of dopamine neuron distinctly convey positive and negative motivational signals. Nature *459*, 837–841.

Matsumoto, M., and Takada, M. (2013). Distinct representations of cognitive and motivational signals in midbrain dopamine neurons. Neuron *79*, 1011–1024.

McDevitt, R.A., Tiran-Cappello, A., Shen, H., Balderas, I., Britt, J.P., Marino, R.A.M., Chung, S.L., Richie, C.T., Harvey, B.K., and Bonci, A. (2014). Serotonergic versus nonserotonergic dorsal raphe projection neurons: differential participation in reward circuitry. Cell Rep. *8*, 1857–1869.

Mirenowicz, J., and Schultz, W. (1996). Preferential activation of midbrain dopamine neurons by appetitive rather than aversive stimuli. Nature *379*, 449–451.

Miyamichi, K., Shlomai-Fuchs, Y., Shu, M., Weissbourd, B.C., Luo, L., and Mizrahi, A. (2013). Dissecting local circuits: parvalbumin interneurons underlie broad feedback control of olfactory bulb output. Neuron *80*, 1232–1245.

Morales, M., and Root, D.H. (2014). Glutamate neurons within the midbrain dopamine regions. Neuroscience *282C*, 60–68.

Phillipson, O.T. (1979). Afferent projections to the ventral tegmental area of Tsai and interfascicular nucleus: a horseradish peroxidase study in the rat. J. Comp. Neurol. *187*, 117–143.

Roeper, J. (2013). Dissecting the diversity of midbrain dopamine neurons. Trends Neurosci. *36*, 336–342.

Root, D.H., Mejias-Aponte, C.A., Zhang, S., Wang, H.-L., Hoffman, A.F., Lupica, C.R., and Morales, M. (2014). Single rodent mesohabenular axons release glutamate and GABA. Nat. Neurosci. *17*, 1543–1551.

Schwarz, L.A., Miyamichi, K., Gao, X.J., Beier, K.T., Weissbourd, B., DeLoach, K.E., Ren, J., Ibanes, S., Malenka, R.C., Kremer, E.J., and Luo, L. (2015). Viral-genetic tracing of the input-output organization of a central noradrenaline circuit. Nature. http://dx.doi.org/10.1038/nature14600.

Soudais, C., Laplace-Builhe, C., Kissa, K., and Kremer, E.J. (2001). Preferential transduction of neurons by canine adenovirus vectors and their efficient retrograde transport in vivo. FASEB J. *15*, 2283–2285.

Stoop, R. (2012). Neuromodulation by oxytocin and vasopressin. Neuron *76*, 142–159.

Swanson, L.W. (1982). The projections of the ventral tegmental area and adjacent regions: a combined fluorescent retrograde tracer and immunofluorescence study in the rat. Brain Res. Bull. *9*, 321–353.

Takatoh, J., Nelson, A., Zhou, X., Bolton, M.M., Ehlers, M.D., Arenkiel, B.R., Mooney, R., and Wang, F. (2013). New modules are added to vibrissal premotor circuitry with the emergence of exploratory whisking. Neuron *77*, 346–360.

Tan, K.R., Yvon, C., Turiault, M., Mirzabekov, J.J., Doehner, J., Labouèbe, G., Deisseroth, K., Tye, K.M., and Lüscher, C. (2012). GABA neurons of the VTA drive conditioned place aversion. Neuron *73*, 1173–1183.

Taniguchi, H., He, M., Wu, P., Kim, S., Paik, R., Sugino, K., Kvitsiani, D., Fu, Y., Lu, J., Lin, Y., et al. (2011). A resource of Cre driver lines for genetic targeting of GABAergic neurons in cerebral cortex. Neuron *71*, 995–1013.

Tsai, H.-C., Zhang, F., Adamantidis, A., Stuber, G.D., Bonci, A., de Lecea, L., and Deisseroth, K. (2009). Phasic firing in dopaminergic neurons is sufficient for behavioral conditioning. Science *324*, 1080–1084.

Ungless, M.A., Magill, P.J., and Bolam, J.P. (2004). Uniform inhibition of dopamine neurons in the ventral tegmental area by aversive stimuli. Science *303*, 2040–2042.

Watabe-Uchida, M., Zhu, L., Ogawa, S.K., Vamanrao, A., and Uchida, N. (2012). Whole-brain mapping of direct inputs to midbrain dopamine neurons. Neuron *74*, 858–873.

Weissbourd, B., Ren, J., DeLoach, K.E., Guenthner, C.J., Miyamichi, K., and Luo, L. (2014). Presynaptic partners of dorsal raphe serotonergic and GABAergic neurons. Neuron *83*, 645–662.

Wickersham, I.R., Lyon, D.C., Barnard, R.J.O., Mori, T., Finke, S., Conzelmann, K.-K., Young, J.A.T., and Callaway, E.M. (2007). Monosynaptic restriction of transsynaptic tracing from single, genetically targeted neurons. Neuron *53*, 639–647.

Wise, R.A., and Rompré, P.-P. (1989). Brain dopamine and reward. Annu. Rev. Psychol. *40*, 191–225.

Zahm, D.S., Cheng, A.Y., Lee, T.J., Ghobadi, C.W., Schwartz, Z.M., Geisler, S., Parsely, K.P., Gruber, C., and Veh, R.W. (2011). Inputs to the midbrain dopaminergic complex in the rat, with emphasis on extended amygdala-recipient sectors. J. Comp. Neurol. *519*, 3159–3188.

Zweifel, L.S., Fadok, J.P., Argilli, E., Garelick, M.G., Jones, G.L., Dickerson, T.M.K., Allen, J.M., Mizumori, S.J.Y., Bonci, A., and Palmiter, R.D. (2011). Activation of dopamine neurons is critical for aversive conditioning and prevention of generalized anxiety. Nat. Neurosci. *14*, 620–626.

Cell

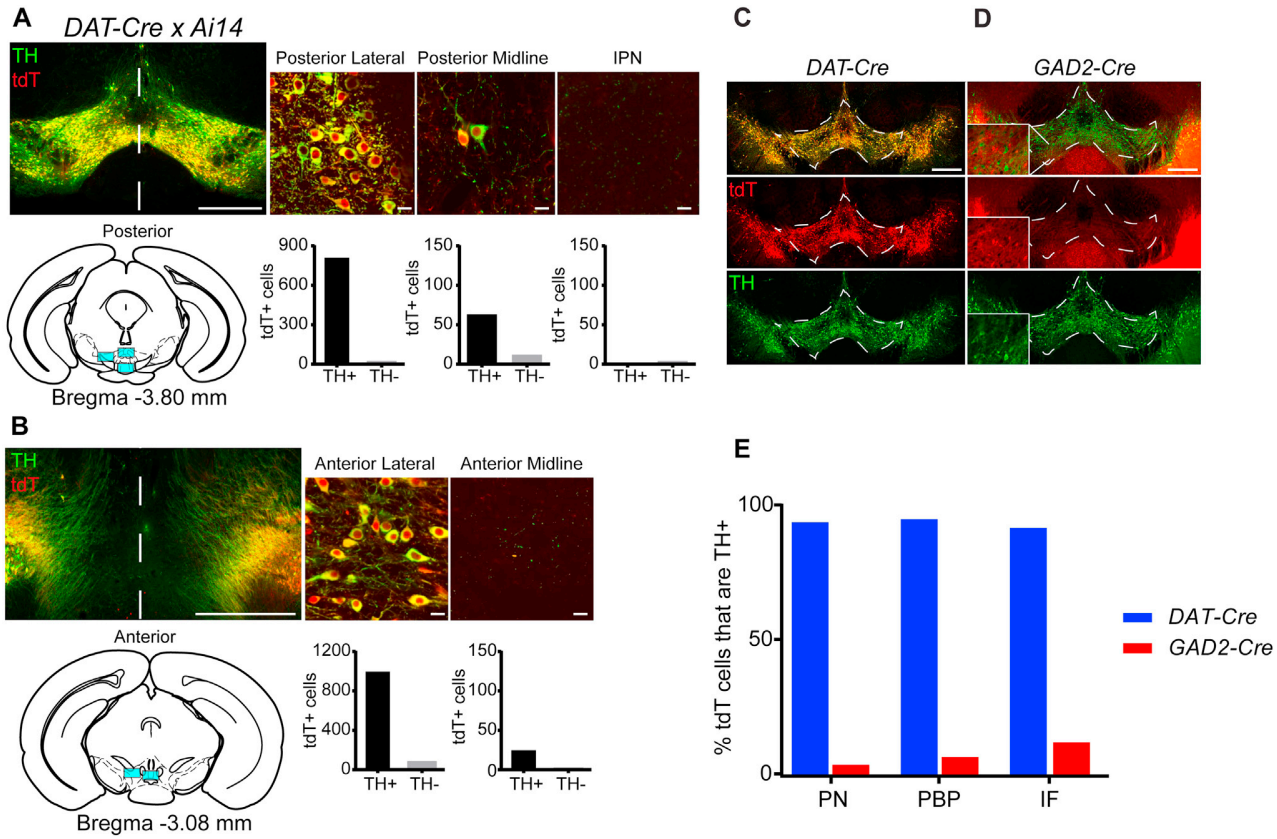

Figure S1. Characterization of *DAT-Cre* and *GAD2-Cre* Expression in the Ventral Midbrain, Related to Figure 1

(A and B) *DAT-Cre* was crossed to the *Ai14* Cre reporter line, which expresses tdTomato in all cells with a Cre expression history. Sections were stained with a tyrosine hydroxylase (TH) antibody, and tdTomato$^+$/TH$^+$ cells were quantified in five regions: two in the anterior of the VTA, and three in the posterior. These five regions are shown by the blue windows on the coronal atlas section. The low-magnification images on the left highlight the overall overlap between tdTomato and TH, while the higher-magnification images on the right show a subset of cells in each window. Dashed lines indicate the midline. Quantification of overlap is provided in the bar graphs below each image. Four 50-μm sections were quantified for both anterior and posterior regions. n = 2 mice for each condition. Scale, 500 μm (low mag); 20 μm (high mag).

(C and D) Ventral midbrain expression of two Cre lines used in this study, *DAT-Cre* (C) and *GAD2-Cre* (D), as reported by the tdTomato Cre reporter *Ai14*. While neurons expressing *DAT-Cre* are largely limited to the VTA and SNc, multiple regions in the ventral midbrain, including the VTA, express *GAD2-Cre*. Dashed lines indicate boundaries of the VTA. Inset, high magnification image of tdTomato$^+$ TH$^-$ neurons in the VTA. Scale, 500 μm.

(E) The percentage of neurons co-staining with the TH antibody in the VTA was quantified in *DAT-Cre* and *GAD2-Cre* mice. The VTA was subdivided into three regions: the paranigral nucleus (PN), parabrachial pigmented nucleus (PBP), and interfascicular nucleus (IF). n = 2 mice for each condition.

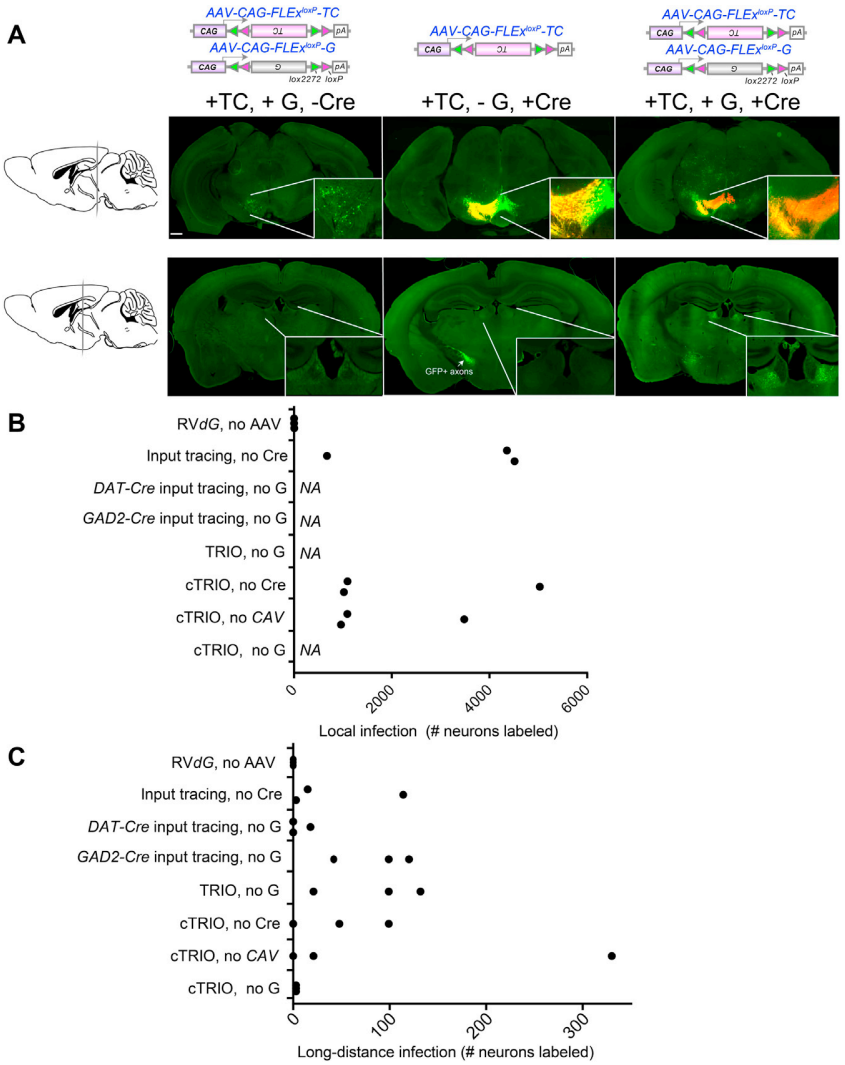

Figure S2. Control Experiments for Rabies Tracing, TRIO, and cTRIO, Related to Figures 1, 3, and S3

(A) A sample input tracing experiment (right panels) with two controls (left and middle panels). In the first control, AAVs were injected into the VTA in a wild-type animal, where there was no Cre to permit Cre-dependent TC or G expression (left). The second control omitted *AAV$_8$-CAG-FLEx^{loxP}-G* (middle). RV*dG* (not depicted) was subsequently injected in all experiments. Local infections are shown in the upper row in coronal sections through the VTA, while representative long-distance inputs are shown in the lower row in coronal sections through the lateral habenula (LHb). In the first control, there are scattered local GFP$^+$ cells, which are most likely due to low-level Cre-independent leaky TC expression that is not sufficient for mCherry to be detected but sufficient for RV*dG* infection due to high sensitivity of TC (Miyamichi et al., 2013). In the second control, many TC$^+$ (red) RV*dG*-GFP$^+$ (green) cells were visible at the injection site. In both cases, less than 0.3% of the long-distance GFP$^+$ cells that were detected in experimental mice (Cre$^+$ and G$^+$) were detected in these control mice. When both TC and G were supplied by AAV injection into a *DAT-Cre* mouse (right panel), many thousands of long-distance inputs were labeled (see Table S1). Scale, 500 μm.

(B) Quantification of local infections (from bregma, posterior 2.7 to 3.9 mm) in control mice. *NA* represents hundreds to thousands of yellow cells at the injection site, so the number of local infection events was not quantified. Although experimental mice for input tracing, TRIO, and cTRIO typically contain several fold more GFP$^+$ cells within the same local areas (coronal sections between 2.7 and 3.9 mm posterior to bregma), we excluded these local areas for quantifications for input tracing, TRIO, and cTRIO.

(C) Quantification of long-distance background infection in various control conditions.

In panels B and C, the first row corresponds to a rabies tracing control where no AAV was injected, testing pseudotyping efficiency. The next four rows are controls for input tracing and TRIO, where either Cre or G was omitted. The last three rows are cTRIO controls, where Cre, CAV, or G was omitted. Dots represent individual experiments. For controls exhibiting > 50 long-distance background infection events, > 70% of these labeled neurons were located in the habenula. n = 3 for each control experiment.

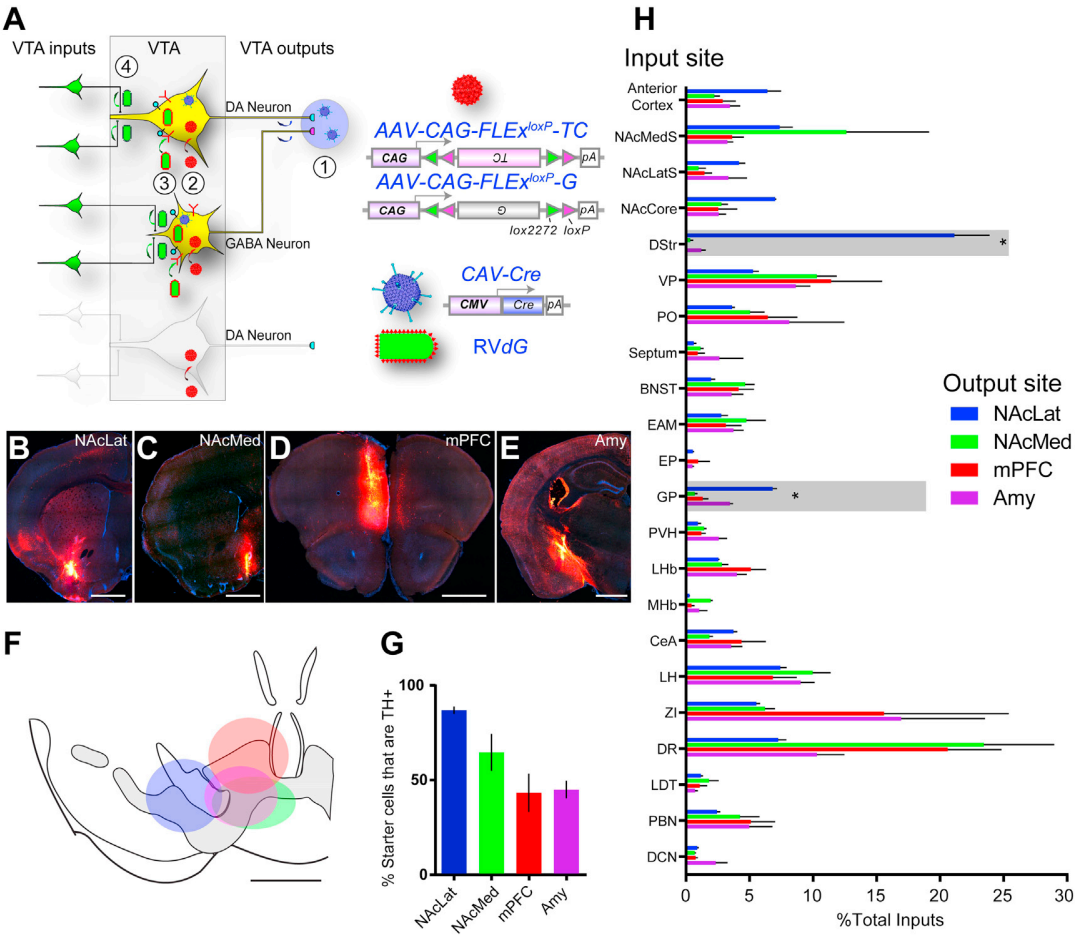

Figure S3. TRIO Analysis of VTA Input-Output Relationships, Related to Figure 3

(A) Schematic of TRIO experiments. (1) *CAV-Cre* was injected into one of four output sites. (2) On the same day, AAVs expressing Cre-dependent TC and G were injected into the VTA. (3) Two weeks later, RV*dG* was injected into the VTA. (4) Five days were permitted for rabies transmission to input neurons before histological analysis.

(B–E) Representative images of CAV injection at four output sites as indicated. Here *CAV-Cre* was injected into the tdTomato Cre reporter line *Ai14*. As neurons near the injection sites as well as those projecting axons to the injection sites are labeled by tdTomato, whereas the co-injected green retrobeads are more concentrated at the injection site, the green fluorescence signals (yellow as they overlap with red signals from tdTomato) are better indicators of the injection sites. Scale, 1 mm.

(F) Coronal section in the VTA indicating the position of starter cell distributions. Each oval indicates the combination of all starter cells across each of four brains for a TRIO condition, with the size of each oval centered at the center of mass of the starter cells, and representing one standard deviation in both the medial–lateral and dorsal–ventral dimensions. The center of mass and distribution of starter cells is unique for each condition ($p < 0.001$ for all comparisons using multiple t tests for the medial–lateral or dorsal–ventral axis, followed by Fischer's combined probability test for each pairwise comparison). Scale, 500 μm.

(G) Percentage of starter cells for each condition that co-label with TH. Individual p-values are reported in Table S2.

(H) Whole-brain input data to each of the VTA neuronal populations defined by TRIO ($n = 4$ for each condition). Percentage of total inputs is plotted on the x axis, and brain region on the y axis. Brain regions with significant differences ($p < 0.05$, 1-way ANOVA for each brain region, with Holm-Sidak correction for 22 1-way ANOVAs) are highlighted in gray. *: DStr and GP send significantly different fractional input to NAcLat-projecting VTA-DA neurons compared with NAcMed, mPFC, and Amy-projecting VTA-DA neurons ($p < 0.05$, post hoc pairwise comparisons with Holm-Sidak corrections for 6 comparisons). See Figure 1 for abbreviation of anatomical regions.

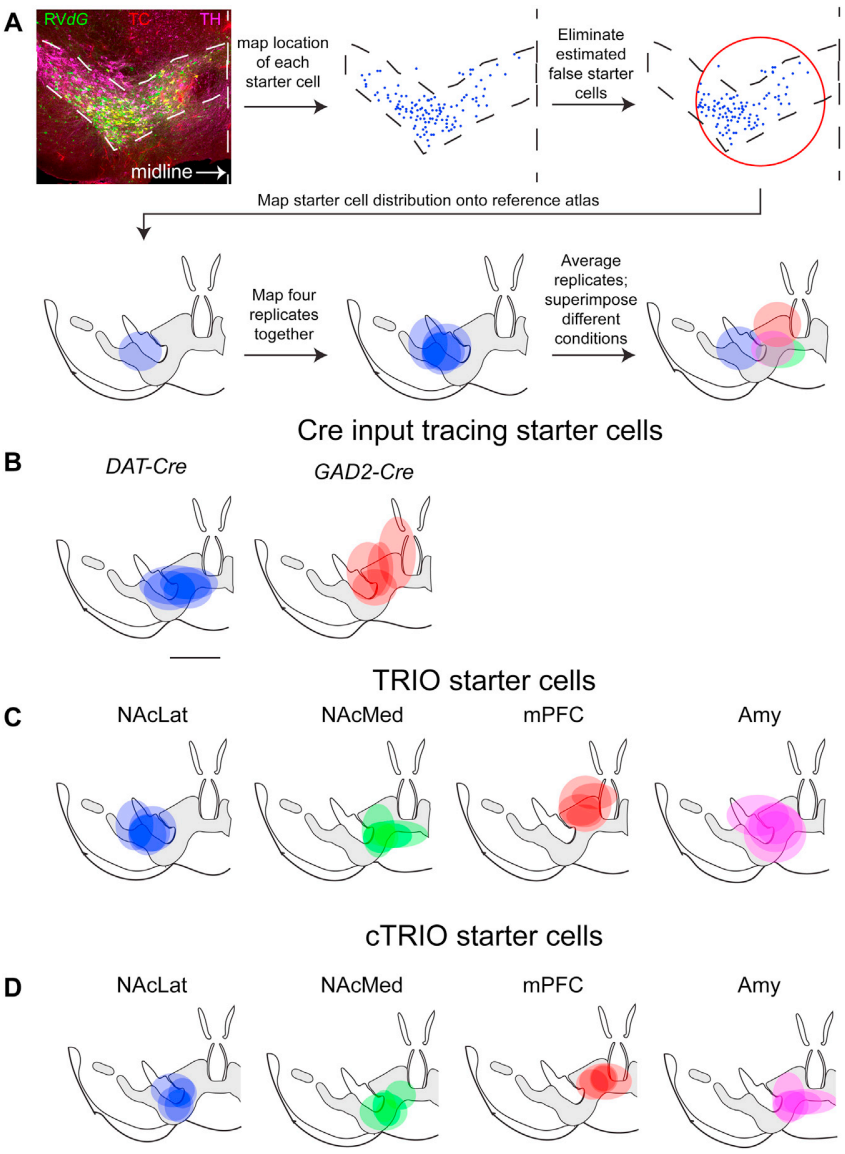

Figure S4. Analysis of Spatial Distribution of Starter Cells, Related to Figures 1, 3, and S3

(A) Schematic summary of the procedure for analyzing spatial distribution of starter cells (see Supplemental Experimental Procedures for details). Top left, a representative image of starter cells in the VTA (between the dotted outline) from a TRIO experiment where *CAV-Cre* was injected into the NAcLat. RV*dG* is shown in green, TC in red, and TH antibody in magenta. For each image, each identified starter cell is registered as a dot (top row, middle). Estimated false starter cells (those that express TC but not G) outside the circle were eliminated (top row, right). The remaining starter cells were registered onto the corresponding atlas section. An oval is used to represent starter cell distribution, with the location of the oval centered at center of mass for starter cells, and the horizontal or vertical radius of the oval representing one standard deviation of starter cell distribution in the x (M–L) or y (D–V) dimension (bottom row, left). The oval for each experiment is then superimposed onto the same atlas section (bottom row, middle). The averages of all experiments for each condition are then plotted onto the same atlas image (bottom row, right), shown in Figures 3C and S3F.

(B–D) Starter cell distribution for input tracing (B), TRIO (C), and cTRIO (D). Each oval represents one experiment, and replicate experiments are represented as superimposed ovals (equivalent to the middle panel in the bottom row of panel A). The output site or Cre line is shown above each schematic. Scale, 500 μm. Table S3 lists coordinates for the center of mass of starter cells for each condition.

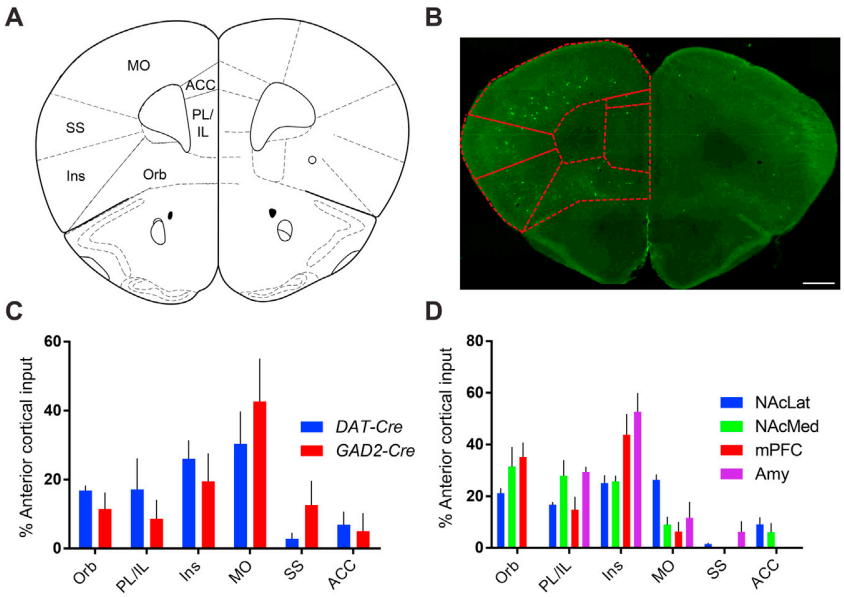

Figure S5. Detailed Analysis of Anterior Cortical Inputs to VTA Neurons, Related to Figures 1 and 5

(A) The anterior cortex was subdivided into six regions: the orbital cortex (Orb), prelimibic/infralimbic cortex (PL/IL), insular cortex (Ins), motor cortex (MO, anterior part only), somatosensory cortex (SS, anterior part only), and anterior cingulate cortex (ACC), and the inputs in each region were quantified.

(B) A sample coronal section of cortical inputs from a *GAD2-Cre* animal.

(C) The percentage of inputs from each cortical region as a fraction of the total anterior cortical (AC) inputs was quantified for *DAT-Cre* and *GAD2-Cre* animals. Total neurons counted: *DAT-Cre* = 828 (n = 4), *GAD2-Cre* = 786 (n = 4).

(D) The same analysis was done for cTRIO experiments in *DAT-Cre* animals. Total neurons counted: NAcLat = 6012 (n = 4), NAcMed = 630 (n = 4), mPFC = 120 (n = 4), Amy = 48 (n = 3). Scale, 500 μm.

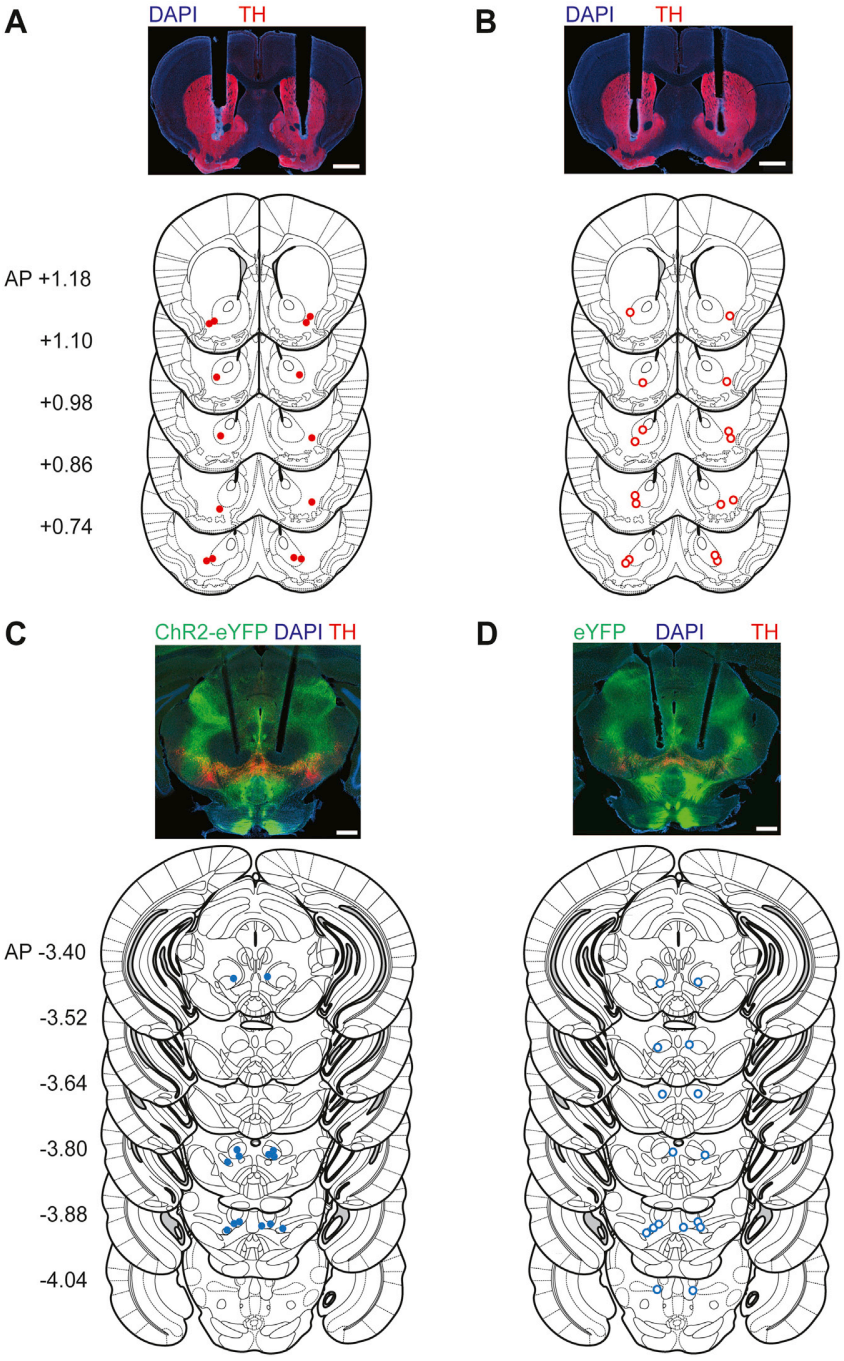

Figure S6. Histological Verification of Drug Cannulae and Optical Fiber Placements for Mice Used in Behavioral Experiments, Related to Figure 6

(A) Location of drug infusion cannulae in mice injected with ChR2-eYFP virus. Top, example cannula placement from a representative ChR2-eYFP-expressing mouse. Scale, 1 mm. Bottom, infuser tip placements in all ChR2-eYFP mice (n = 7, solid red circles).

(B) Same as in A, but for eYFP-expressing control mice (n = 8). Open red circles indicate infuser tip placement in this group.

(C) Location of optical fibers in mice injected with ChR2-eYFP virus. Top, example optical fiber placement from a representative ChR2-eYFP-expressing mouse. Scale, 500 μm. Bottom, optical fiber placements in all ChR2-eYFP mice (n = 7, solid blue circles).

(D) Same as in C, but for eYFP-expressing control mice (n = 8). Open blue circles indicate optical fiber tip placement in this group.

Cell

Supplemental Information

Circuit Architecture of VTA Dopamine Neurons Revealed by Systematic Input-Output Mapping

Kevin T. Beier, Elizabeth E. Steinberg, Katherine E. DeLoach, Stanley Xie, Kazunari Miyamichi, Lindsay Schwarz, Xiaojing J. Gao, Eric J. Kremer, Robert C. Malenka, and Liqun Luo

SUPPLEMENTAL EXPERIMENTAL PROCEDURES

DNA Constructs

AAV-CAG-FLEx^{loxP}-G, *AAV-CAG-FLEx^{loxP}-TC*. *pAAV-CAG-FLEx^{FRT}-G, pAAV-CAG-FLEx^{FRT}-TC*, and *CAV-FLEx^{loxP}-Flp* were constructed as reported previously (Schwarz et al., 2015).

pAAV-hSyn1-FLEx^{FRT}-mGFP (pAAV-hSyn1-FLEx^{FRT}-mGFP-2A-synaptophysin-mRuby) was also constructed using standard molecular cloning methods. GFP was PCR amplified from *pCAG-GFP* (addgene #11150), with primers designed to append the palmitoylation site from GAP43 for membrane targeting to the 5' end of the gene. The 5' primer contained an AscI site, and 3' primer contained the 5' part of a T2A sequence. Synaptophysin-mRuby (gift from Paul Temkin) was PCR amplified using a 5' primer containing the 3' part of a T2A sequence with 20 base pair overlap with the mGFP fragment, and 3' primer containing a SalI site. These fragments were then combined, and a single insert containing mGFP-2A-synaptophysin-mRuby was constructed using the 5' mGFP primer 2 and 3' synaptophysin-mRuby primers. This fragment was then subcloned into the SalI and AscI sites of *pAAV-CAG-FLEx^{FRT}-TC* (to make *pAAV-CAG-FLEx^{FRT}-mGFP-2A-synaptophysin-mRuby*). Primers were as follows:

5' mGFP primer 1:
GAACCAAACAGGTTGAAAAGAATGATGAGGACCAAAAGATCATGGTGAGCAAGGGC
GAGGAG
5' mGFP primer 2:
CTATACGAAGTTATAGGCGCGCCACCATGCTGTGCTGTATGAGAAGAACCAAACAGGT
TGAAAAG
3' mGFP:
CCACGTCGCCGCAGGTCAGCAGGCTGCCCCTGCCCTCCTTGTACAGCTCGTCCATGC
5' synaptophysin-mRuby:
GCTGACCTGCGGCGACGTGGAGGAGAACCCCGGCCCCATGGACGTGGTGAATCAGC
TG
3' synaptophysin-mRuby:
GCTATACGAAGTTATGTCGACTTACCCTCCGCCCAGGCCGGCGAAC

Once completed, the *FLEx^{FRT}* cassette was PCR amplified from *pAAV-CAG-FLEx^{FRT}-mGFP-2A-synaptophysin-mRuby*, and subcloned into the BamHI and EcoRI sites of *pAAV-hSyn1-mCherry* (gift from Michael Lochrie) to make *pAAV-hSyn1-FLEx^{FRT}-mGFP-2A-synaptophysin-mRuby*. Primers used were as follows:

5' FLEx^{FRT}: AGTCGAGAAGGTACCGGATCCTGTGCTGTCTCATCATTTTGG
3' FLEx^{FRT}: GATAAGCTTGATATCGAATTCATCGATCGGCCGCATATAA.

Viral Tracing

For rabies tracing, 100 nL of a 1:1 volume mixture of *AAV$_5$-CAG-FLEx^{loxP}-TC and AAV$_8$-CAG-FLEx^{loxP}-G* was injected into the VTA of 4-6 week old mice. Two weeks later, RV*dG* was injected into the same brain location. After recovery, mice were housed in a BSL2 facility for 5 days to allow for rabies spread and GFP expression.

For TRIO experiments, the same procedure was performed as above, except that *CAV-Cre* was also injected into a VTA output site and 500 nL of a 1:1 volume mixture of *AAV$_5$-CAG-FLEx^{loxP}-TC* and *AAV$_8$-CAG-FLEx^{loxP}-G* was injected into the VTA of wild-type mice.

For cTRIO, *CAV-FLEx^{loxP}-Flp* was injected into a VTA output site, and 500 nL of a 1:1 volume mixture of *AAV$_5$-CAG-FLEx^{FRT}-TC* and *AAV$_8$-CAG-FLEx^{FRT}-G* was injected into the

VTA of *DAT-Cre* mice.

For axon arborization experiments, *CAV-FLEx^{loxP}-Flp* was injected into a VTA output site, and *AAV$_{DJ}$-hSyn1-FLEx^{FRT}-mGFP* was injected into the VTA of *DAT-Cre* mice.

For injections into VTA output sites for TRIO, cTRIO, and axon arborization experiments, 250 nL of *CAV-Cre* or *CAV-FLEx^{loxP}-Flp* was injected into NAcLat (relative to Bregma and in mm, AP +1.45, LM 1.75, DV –4.0), 250 nL into NAcMed (AP +1.78, L0.4, DV –4.1), 500 nL into CeA (AP –1.43, LM 2.5, DV –4.5), and 1 µL into mPFC (two injections of 500 nL, one at AP +2.15, LM 0.27, DV –2.1 and another at AP +2.15, L0.27, DV –1.6).

The titers of these viruses, based on quantitative PCR analysis, were as follows: *AAV$_5$-CAG-FLEx^{loxP}-TC*, 2.4 x 10^{13} genome copies (gc)/mL; *AAV$_8$-CAG-FLEx^{loxP}-G*, 1.0 x 10^{12} gc/mL; *AAV$_5$-CAG-FLEx^{FRT}-TC*, 2.6 x 10^{12} gc/mL; *AAV$_8$-CAG-FLEx^{FRT}-G*, 1.3 x 10^{12} gc/mL; *AAV$_{DJ}$-hSyn1-FLEx^{FRT}-mGFP*, 2.9 x 10^{13} gc/mL, *CAV-Cre*, 2.5 x 10^{12} gc/mL, *CAV-FLEx^{loxP}-Flp*, 5.0 x 10^{12} gc/mL. The titer of RV*dG* was estimated to be 5.0 x 10^8 colony forming units (cfu)/mL based on serial dilutions of the virus stock followed by infection of the 293-TVA800 cell line.

Histology and Imaging

Animals were transcardially perfused with phosphate buffered saline (PBS) followed by 4% formaldehyde. Brains were dissected, post-fixed in 4% formaldehyde for 12–24 hours, and placed in 30% sucrose for 24–48 hours. They were then embedded in Tissue Freezing media and stored in a –80ºC freezer until sectioning.

For rabies tracing analysis, consecutive 60-µm coronal sections were collected onto Superfrost Plus slides and stained for NeuroTrace Blue (NTB, Invitrogen). For NTB staining, slides were washed 1x5 min in PBS, 2x10 min in PBS with 0.3% Triton X-100 (PBST), incubated for 2–3 hours at RT in (1:500) NTB in PBST, washed 1x20 min with PBST and 1x5min with PBS. Sections were additionally stained with DAPI (1:10,000 of 5 mg/mL, Sigma-Aldrich), which was included in the last PBST wash of NTB staining. Whole slides were then imaged with a 5x objective using a Leica Ariol slide scanner with the SL200 slide loader.

For analysis of DA neuron output, every 60-µm coronal section was collected sequentially into PBS. Sections were washed 2x10 min in PBS and blocked for 2–3 hours at room temperature (RT) in 10% normal goat serum (NGS) in PBST. Primary antibody (chicken anti-GFP, Aves Labs, 1:1000) was diluted in 5% NGS in PBST and incubated for four nights at 4^{o}C. After 3x10 min washes in PBST, secondary antibodies were applied for two nights at 4^{o}C (donkey anti-chicken AlexaFluor488, 1:250, Jackson ImmunoResearch), followed by 3x10min washes in PBST. Sections were additionally stained with DAPI. All images were acquired using a 5x objective on the Leica Ariol slide scanner, and processed using NIH ImageJ software.

For starter cell identification, sections were unmounted after slide scanning, blocked in PBST and 10% NGS for 2–3 hours at room temperature, and incubated in rat anti-mCherry antibody (1:2000, Life Sciences) and rabbit anti-TH antibody (1:1000, Millipore) at 4^{o}C for four nights. After primary antibody staining, sections were washed 3x10 min in PBST, and secondary antibodies (donkey anti-rat Cy3 and donkey anti-rabbit 647, Jackson ImmunoResearch) were applied for two nights at 4^{o}C, followed by 3x10min washes in PBST and remounting. Confocal z-stacks were acquired using a 20x objective on a Zeiss LSM 780 confocal microscope. For Figure S1, imaging and quantification were done as previously described (Lammel et al., 2015).

Data Analysis for Whole-Brain Tracing

The 22 regions chosen for analysis included the major inputs to the VTA that fell outside of the

excluded region near the injection site. For VTA transsynaptic tracing and TRIO/cTRIO analysis, GFP-positive input neurons were manually counted from every third 60-μm section through the entire brain, except near the VTA, as specified in Figure S2 (posterior 2.7 mm to 3.9 mm from bregma). As each brain differed in total numbers of input neurons, we normalized neuronal number in each area by the total number of input neurons counted in the same brain, as previously described (Weissbourd et al., 2014). For 21 brain regions (all except for the LDT), every third section was counted. For the LDT, as the nucleus is small, every other section was counted. If the total number of inputs in a region was less than 5, every section was counted. Counts were then multiplied by the scale factor (3 for most regions, 2 for the LDT). We did not adjust for the possibility of double-counting cells in any of our quantifications, which likely results in slight over-estimates, with the amount of over-estimation depending on the size of the cell in each region quantified (Weissbourd et al., 2014).

Anatomical Regions and Their Abbreviations

For quantifications of brain regions, boundaries were based on the Mouse Brain Atlas in Stereotaxic Coordinates, Franklin and Paxinos, 3rd ed. (Franklin & Paxinos, 2007). The anterior cortex included all cortical regions located anterior to, and including, the first section containing the corpus callosum. Subdivisions of the nucleus accumbens shell (NAcMedS, NAcLatS) were identified primarily on the basis of NeuroTrace staining, and for output tracing, were assisted by DAT antibody staining (rabbit anti-DAT, ab18548, abcam, 1:1000). Other region definitions that included multiple subregions listed in the Franklin-Paxinos atlas, 3rd ed. (Franklin & Paxinos, 2007), are as follows:

AC – anterior cingulate cortex (ACC); infralimbic cortex (IL); insular cortex (Ins); motor cortex (MO; anterior portion); orbital cortex (Orb); prelimbic cortex (PL); somatosensory cortex (SS, anterior portion).

CeA – central amygdala lateral, medial, and capsular nuclei

DR – as defined in Weissbourd et al., 2014.

EAM – extended amygdala, anterior amygdaloid area

LDT – laterodorsal tegmental area, dorsomedial tegmental area, dorsal tegmental nucleus, Barrington's nucleus, ventral tegmental nucleus, subpeduncular tegmental nucleus

PO – medial preoptic area, lateral preoptic area, lateral anterior hypothalamic area, anterior hypothalamic area, striohypothalamic nucleus

Septum – triangular septal nucleus, lateral septum, dorsal fornix, septofimbrial nucleus, medial septum, septohypothalamic nucleus, septohippocampal nucleus, lambdoid septal zone

VP –interstitial nucleus of posterior limb of anterior commissure (IPAC), substantia innominata, horizontal diagonal band, nucleus of the vertical diagonal band

Abbreviations for brain regions made throughout the paper are listed below, in alphabetical order:

AC – anterior cortex

BNST – bed nucleus of the stria terminalis

CeA – central amygdala

DCN – deep cerebellar nucleus

DR – dorsal raphe

DStr – dorsal striatum

EAM – extended amygdala

EP – entopeduncular nucleus (GPi)
GP – globus pallidus (GPe)
LDT – laterodorsal tegmentum
LH – lateral hypothalamus
LHb – lateral habenula
MHb – medial habenula
NAcCore- nucleus accumbens, core
NAcMedS – nucleus accumbens, medial shell
NAcLatS – nucleus accumbens, lateral shell
PBN – parabrachial nucleus
PO – pre-optic area
PVH – paraventricular hypothalamus
VP – ventral pallidum
VTA – ventral tegmental area
ZI – zona incerta

Rabies Tracing Combined with In Situ Hybridization (ISH)
For each input region, we alternated sections between probes, with an average of every 2nd section with the same probe in the PVH and LH, and every 4th section for the DR. The brain regions analyzed conform to the regions defined as in Mouse Brain Atlas in Stereotaxic Coordinates, Franklin and Paxinos, 3rd ed. (Franklin & Paxinos, 2007), except for the DR, which was as previously defined (Weissbourd et al., 2014). Sections covered the whole region expressing the relevant gene in the region being analyzed.

PCR Primers for ISH Probes
The probes for oxytocin, vasopressin, vGluT1/2/3, and GAD1/2 are the same as used previously (Weissbourd et al., 2014). For the other probes, the following primers were used to amplify the templates for ISH probes. T3 polymerase recognition site is indicated by underline.

Neurotensin
5'-AGAAGAAGATGTGAGAGCCCTG
5'-AATTAACCCTCACTAAAGGGCTGCTTTGGGTTAATAACGCTC
Orexin
5'-CTGCTGCTGCTGCTACTGCT
5'-AATTAACCCTCACTAAAGGGGGGAAGTTTGGATCAGGACA
Tph2
5'-GTATTGAGAATGTGGTGCAGGA
3-AATTAACCCTCACTAAAGGGCACTCAGTCTACATCCATCCCA
Tyrosine Hydroxylase
5'-GATTGCAGAGATTGCCTTCC
5'-AATTAACCCTCACTAAAGGGCCTGTGGGTGGTACCCTATG

Axon Arborization Analysis
After sectioning and antibody staining, sections were mounted and imaged, as for input tracing analysis. For each region, five 60-μm sections were chosen for analysis from within a defined anterior-posterior segment (all coordinates are relative to bregma in mm): anterior 1.41 to 0.85

for nucleus accumbens and striatum, 0.37 to 0.01 for BNST and VP, 1.87 to 1.53 for mPFC, and posterior 0.95 to 1.79 for the CeA. For the septum, 10 sections were analyzed, 5 each from 1.41 to 0.85 and 0.37 to 0.01. The entire regions within each section were taken, and boundaries were defined based on DAPI staining and on the Franklin and Paxinos mouse brain atlas, 3rd ed. (Franklin & Paxinos, 2007). For analysis, the background was first subtracted, and the mean of local background after subtraction was multiplied by a constant value (4, for all but one sample targeting NAcLat-projecting neurons that had sparser labeling, where a value of 3 was used). This value was then set as the threshold, with pixels above this gray-scale value being interpreted as positive signal from VTA-DA neuron axons. The threshold value was kept constant for all sections analyzed within a brain. The total area and area fraction covered by the above-threshold axon signal was measured for each region and averaged across the 5 (or 10) sections.

Analysis of Spatial Distribution of Starter Cells in the VTA

To assess the spatial distribution of starter cells in our experiments, nine 60-μm coronal sections through the VTA were quantified (corresponding to one tissue section per atlas section in the Franklin and Paxinos Atlas). These sections were collected in order through the VTA of experimental animals and processed as described above in Histology and Imaging. Starter cells were considered as all cells that were both GFP^+ and TC^+. The location of these cells was manually mapped onto digital reference images from the Franklin and Paxinos atlas using the Cell Counter plugin in ImageJ. x, y, and z coordinates were obtained for each starter cell in each experiment. Diagrams displaying the spatial distribution of starter cells (Figure 3C, S3F, S4) are collapsed along the anterior–posterior (z) axis, and therefore underestimate the true distinction in spatial distribution of starter neurons. The spatial distribution for the starter cells was calculated for the x and y dimensions separately.

As we injected two AAVs to express TC and G separately, it was possible that some cells expressed one gene, but not the other. Cells that expressed TC, but not G, would therefore appear red and green and would be considered a starter cell, but as they would lack expression of G, no inputs would be labeled from these "false" starter cells. Corrections for false starter cells were made using the observed spread of *AAV_5-CAG-FLEx^{loxP}-TC* and *AAV_8-CAG-FLEx^{loxP}-G*. Native mCherry fluorescence was used to visualize TC; for G, 60-μm tissue sections were stained for the rabies glycoprotein (mouse anti-rabies glycoprotein, Millipore, 1:500, followed by donkey anti-mouse AlexaFluor488, 1:500, Jackson ImmunoResearch). The distance from the targeted center of the injection site in the VTA to the edge of observed fluorescence for three sections located near the injection site, and three sections located approximately 600 μm posterior to the injection site was quantified. False starter cells were considered as those that expressed TC, but not G. The Euclidian distance from the center of injection to the edge of spread was then calculated for each AAV, and as the radius of spread from the injection site as visualized in both anterior and posterior sections approximated a sphere, a virtual sphere was created with a radius equal to the spread distance of *AAV_8-CAG-FLEx^{loxP}-G* (which was smaller than that of *AAV_5-CAG-FLEx^{loxP}-TC*). These values (for either 0.1 μL, in the case of *DAT-Cre* and *GAD2-Cre* input tracing, or 0.5 μL, for TRIO and cTRIO) were then used to exclude starter cells that were located outside of the sphere of TC and G co-expression. The false starter cell correction, as well as the center of mass (CoM; the mean location of starter cells) and standard deviation of the starter cell spatial distribution calculations were made using custom MATLAB code based on the x, y, and z coordinates for each starter cell.

For input quantification, not every section was counted for starter cell counting: while the

VTA spanned about twenty sections of 60-μm thickness, only nine sections containing the VTA were quantified, as this corresponded to the number of unique sections containing the VTA that are represented in the Franklin and Paxinos atlas. In this way, starter cells from one 60 μm section would correspond to one digital image. Therefore, when total numbers of starter cells were reported (Table S1), the total number of starter cells for each brain was multiplied by 20/9.

Electrophysiological Recordings from Adult Mouse Midbrain Slices

Mice were deeply anaesthetized with pentobarbital (200 mg/kg ip; Ovation Pharmaceuticals, Deerfield, IL). Coronal midbrain slices (200 μm) were prepared after intracardial perfusion with ice-cold artificial cerebrospinal fluid (ACSF) containing elevated sucrose (in mM): 50 sucrose, 125 NaCl, 25 $NaHCO_3$, 2.5 KCl, 1.25 NaH_2PO_4, 2.5 $CaCl_2$, 1.2 $MgCl_2$, and 2.5 glucose (oxygenated with 95% O_2/5% CO_2). After 60 min of recovery, slices were transferred to a recording chamber and perfused continuously at 2–4 ml/min with oxygenated ACSF (22.5 mM sucrose) at 30 ºC. Picrotoxin (50 μM, Sigma) was added to block inhibitory currents mediated by $GABA_A$ receptors. Patch pipettes (3.8-4.4 MΩ) were pulled from borosilicate glass (G150TF-4; Warner Instruments) and filled with internal solution containing (in mM): 117 $CsCH_3SO_3$, 20 HEPES, 0.4 EGTA, 2.8 NaCl, 5 TEA, 4 MgATP, 0.3 NaGTP, 5 QX314, and 0.1 Spermine (pH 7.3, 270–285 mOsm). Labeled DA neurons were visualized by infrared-differential interference contrast (IR-DIC) video microscopy and epifluorescence (Olympus) for detection of retrobeads (red) and GFP.

Labeled DA neurons were visualized with a 40X water-immersion objective on an upright fluorescent microscope (BX51WI; Olympus) equipped with infrared-differential interference contrast video microscopy and epifluorescence (Olympus) for detection of retrobeads. ChR2 was stimulated by flashing 473 nm light (2-ms pulses; 0.1 Hz; 12 mW) through the light path of the microscope using an ultrahigh-powered light-emitting diode (LED) powered by an LED driver (Prizmatix, Modiin Ilite) under computer control. The light intensity of the LED was not changed during the experiments and the whole slice was illuminated. A dual lamp house adaptor (Olympus) was used to switch between the fluorescence lamp and LED light source

A total of 13 mice were used for recording experiments (5 for mPFC, 5 for LHb, and 3 for anterior cortex).

Behavioral Experiments

Subjects: 15 male C57Bl/6J mice (Jackson Laboratories, #664), 8–10 weeks old at the start of the experiment, were group-housed in a light-regulated colony room (12 hr light/dark cycle; lights on at 7:00 am). Food and water were available *ad libitum* throughout the experiment.

Surgical procedures for behavioral experiments: Standard stereotaxic procedures were used to infuse virus, and implant optical fibers and guide cannulae in two separate surgeries under ketamine/dexmedetomidine anesthesia. All coordinates are relative to skull surface and bregma in mm. In the first surgery, *AAV_5-hsyn1-eYFP* (n=8) or *AAV_5-hsyn1-ChR2-eYFP* (n=7) (UNC viral vector core, $3.5x10^{12}$ and $4.6x10^{10}$ gc/ml, respectively) was infused into 4 separate sites (2 per hemisphere) in the anterior cortex. Coordinates for viral injections were as follows: AP +2.1; ML ± 2.2; DV –2.1; 0.3 μL and AP +1.95; ML ± 0.3; DV –2.1; 0.2 μL. Virus was delivered at a rate of 0.1 μL/min and the injection needle was left in place for 5 minutes after each infusion before it was slowly removed. Following surgery, mice were returned to group housing after being allowed to recover on a heating pad. 8 weeks later, mice underwent a second surgery to

implant optical fibers (made in-house with 0.39 NA, 200 μm diameter optical fiber, Thorlabs) targeted just dorsal to the VTA and guide cannulae (26 ga, Plastics One) targeted to the lateral NAc. The following coordinates were used: optical fibers; AP –3.1; ML ± 1.2; DV –4.1; 10° angle within the coronal plane and cannulae; AP +1.45; ML ± 1.55; DV –3.0; no angle. Implants were secured to the skull with metal screws (Antrin Miniature Specialists) and Geristore dental epoxy (DenMat). Although only used for drug infusions in ChR2-eYFP-expressing mice, all mice received cannula implants in order to maintain consistency between groups. Following the second surgery mice were single-housed for the remainder of the experiment. Mice were allowed to recover for >10d before behavioral procedures commenced.

Behavioral apparatus: Experimental sessions were conducted in operant conditioning chambers (24 cm W x 20 cm D x 18 cm H, Med Associates Inc.) contained within sound-attenuating cubicles. The left side of the chamber was fitted with 5 nosepoke ports, each with an LED light at the rear. A video camera (Med Associates Inc.) was positioned at the top of the sound-attenuating cubicle that provided a top-down view of the entire conditioning chamber. Offline video analysis with tracking software (Biobserve) allowed locomotion—measured as total distance traveled during the 1hr session—to be quantified during some training sessions. Prior to behavioral sessions, mice were gently attached to patch cables made in-house with optical fiber (0.39 NA, 200 μm diameter, Thorlabs) via a ceramic split sleeve (Precision Fiber Products). The patch cables were also connected to bilateral rotary joints (Doric Lenses), which permitted free rotation while transmitting blue light from an upstream 473 nm blue laser (Laserglow). Optical stimulation was controlled by a computer running Med PC IV software (Med Associates Inc.), which also recorded responses at all nosepoke ports and initiated and terminated video recording.

ICSS acquisition: Prior to the first behavioral session, mice were familiarized with cereal treats (Fruit Loops, Kellogg) in their home cage. On the first training day, all nosepokes were baited with crushed cereal treats to facilitate initial investigation. The start of the session was indicated to the mouse by the illumination of a white house light. Session length was 60 min, during which time mice were free to respond at any nosepoke port. 4 ports were designated "active" ports, and a response at these ports produced 2s of optical stimulation at a particular frequency (1, 5, 10 or 20 Hz); the LED at the back of the corresponding port was concurrently illuminated to provide a visual cue signaling the presence of optical stimulation. Responses made within the 2s stimulation period were recorded but had no consequence. Responses at a 5th "inactive" nosepoke port were recorded but did not result in either optical stimulation or cue light presentation. Testing occurred once per day for 5 days. Peak light output during photostimulation was estimated to be ~2.75 mW at the tip of the implanted fiber (~22 mW/mm^2), and ~5 mW/mm^2 at the targeted tissue 200 μm from the fiber tip. The power density estimates were based on the light transmission calculator at www.optogenetics.org/calc.

Drug infusions: A subset of high-responding mice from the ChR2-eYFP group (n=5) was used for drug infusion studies. These mice received 4 additional ICSS training sessions prior to the initiation of drug infusions in order to establish baseline response rates. On infusion days, mice received bilateral 0.25 μL infusions of either flupenthixol (F114, Sigma, dissolved in saline) or saline vehicle via a 33 ga infusion cannula (Plastics One) that was inserted into the implanted guide cannula and extended a further 1.5 mm into the brain, for a final depth of 4.5 mm below skull surface. Infusions were made at a rate of 0.25 μL/min with a syringe pump (Harvard

Apparatus), and the infusion cannula was left in place for an additional minute to permit drug diffusion. After each infusion, mice were returned to their home cage for 10 minutes to allow drugs to take effect before behavioral sessions began. Behavioral sessions where flupenthixol was administered were always preceded by at least one sham infusion session (where all infusion procedures were followed except that the infusion cannula was cut so as not to project past the end of the guide cannula, and no liquid was infused) and a saline infusion session. Three saline infusion sessions were conducted in total (24 hrs before each flupenthixol infusion); responding in these sessions was equivalent (1-way repeated measures ANOVA, $p>0.05$) so data from these sessions were averaged to yield a single saline measurement.

Histology for mice used for behavioral studies: Mice were deeply anesthetized with sodium pentobarbital and perfused transcardially with 4% paraformaldehyde. Mice were perfused with infusion cannulae inserted into guide cannulae to facilitate post-hoc identification of infuser tip placement. Brains were removed, post-fixed for 24 hours, and sectioned at room temperature on a vibratome. Free-floating 60-µm coronal sections were then processed for TH immunohistochemistry. Sections containing the VTA were also processed for eYFP immunohistochemistry. Sections were incubated in a blocking solution containing bovine serum albumin and Triton X-100 (each 0.2%) in PBS for 20 min. Normal donkey serum (NDS) (10%) was added to blocking solution for a further 30 min incubation. Sections were then incubated overnight with primary antibodies diluted in blocking solution. Following 3 washes with blocking solution, sections were incubated in PBS containing 2% NDS for 10 minutes. Sections were then incubated for 2 hours with secondary antibodies diluted in PBS, washed with PBS several times, mounted on microscope slides in phosphate-buffered water, and coverslipped with Fluoromount G mounting medium containing DAPI nuclear counterstain (Southern Biotech). Concentrations and sources for antibodies were as follows: rabbit anti-TH 1:1500 (Millipore, #AB152), sheep anti-GFP 1:3000 (Novus Biologicals, NB110-75114), donkey anti-rabbit AlexaFluor647 and donkey anti-sheep AlexaFluor488, both 1:200 (Invitrogen). Sections were visualized on a Nikon A1 confocal microscope to determine optical fiber and cannula placements. Although optical fiber and cannula placement varied slightly between animals (see Figure S6), no subjects were excluded.

Data Analysis: Behavioral data were analyzed with SigmaStat software. Parametric tests (one-way repeated measures ANOVA followed by Holm-Sidak post-hoc tests) were used in cases where data met assumptions of normality and equal variance. In cases where data did not meet these assumptions, non-parametric tests (Friedman's repeated-measures ANOVA on ranks followed by Tukey post-hoc tests for within-group comparisons; Mann-Whitney rank sum tests with Bonferroni correction for between-group comparisons) were used.

SUPPLEMENTAL REFERENCES

Franklin, K.B.J. and Paxinos, G. (2007). *The Mouse Brain in Stereotaxic Coordinates*, 3rd Ed. Elsevier, Academic Press, San Diego.

Lammel, S., Steinberg, E. E., Foldy, C., Wall, N. R., Beier, K., Luo, L., & Malenka, R. C. (2015). Diversity of Transgenic Mouse Models for Selective Targeting of Midbrain Dopamine Neurons

Matters Arising Diversity of Transgenic Mouse Models for Selective Targeting of Midbrain Dopamine Neurons. *Neuron*, *85*, 429–438.

Miyamichi, K., Shlomai-Fuchs, Y., Shu, M. M., Weissbourd, B. C., Luo, L., & Mizrahi, A. (2013). Dissecting local circuits: parvalbumin interneurons underlie broad feedback control of olfactory bulb output. *Neuron*, *80*(5), 1232–1245.

Schwarz, L.A., Miyamichi, K., Gao, X.J., Beier, K.T., Weissbourd, B., DeLoach, K.E., Ren, J., Ibanes, S., Malenka, R.C., Kremer, E.J., et al. (2015). Viral-genetic tracing of the input–output organization of a central noradrenaline circuit. Nature *doi:10.1038/nature14600*.

Weissbourd, B., Ren, J., DeLoach, K. E., Guenthner, C. J., Miyamichi, K., & Luo, L. (2014). Presynaptic Partners of Dorsal Raphe Serotonergic and GABAergic Neurons. *Neuron*, *83*(3), 645–662.